Current Topics in Crystal Growth Res., 2 (1995)

Growth of wide band gap II-VI compound semiconductors by physical vapor transport

Ching-Hua Su and Yi-Gao Sha[1]

Space Science Laboratory, NASA/Marshall Space Flight Center, Huntsville, Alabama, USA

I. Introduction

The studies on the crystal growth and characterization of II-VI wide band gap compound semiconductors, such as ZnTe, CdS, ZnSe and ZnS, have been conducted over the past three decades. The research was not quite as extensive as that on Si, III-V, or even narrow band gap II-VI semiconductors because of the high melting temperatures as well as the specialized applications associated with these wide band gap semiconductors. In the past several years, major advances in the thin film technology such as molecular beam epitaxy (MBE) and metal organic chemical vapor deposition (MOCVD) have demonstrated the applications of these materials for the important devices such as light-emitting diode [1], laser [2] and ultraviolet detectors [3] and the tunability of energy band gap by employing ternary [4] or even quaternary systems [5] of these compounds. At the same time, the development in the crystal growth of bulk materials has not advanced far enough to provide low price, high quality substrates needed for the thin film growth technology [6].

Crystallization from vapor has various advantages over melt growth. These advantages result mostly from (1) the lower processing temperature involved — the high melting temperatures of these materials, as listed in Table 1 together with their energy band gaps, make the melt growth process very difficult to handle, (2) physical vapor transport acts as a purification process [12] because of the differences in the vapor pressures of the native elements and the impurities, and (3) most solid-vapor interfaces exhibit higher interfacial morphological stability [13] during growth due to their low atomic roughness [14] and, consequently, the pronounced growth rate anisotropy. The technique of physical vapor transport in closed ampoules is especially attractive for space investigation because of its experimental simplicity and minimal needs for complex process control. In this chapter, we will discuss the activities of bulk growth of these wide band gap II-VI semiconductors by physical vapor transport (referred to as PVT hereafter) technique developed in our laboratory during the past years.

The main disadvantage of vapor growth technique compared to other growth technique is that the growth rates are low and the grown crystals are small with variable single crystal yield [6]. While seeded growth technique can be adopted to improve the yield of single crystal the transport process needs to be studied carefully to increase the growth rates. The mechanism of the vapor transport process in II-VI semiconductors is different from those of the IV-VI and II-VII_2 compounds. Under the ideal condition that the partial pressure of the residual (foreign) gas is zero, this difference is mainly caused by the thermodynamic fact that the predominant vapor species in equilibrium with the II-VI compounds in the temperature

[1]Universities Space Research Association.

Table 1. Melting points and energy band gaps of II-VI wide band gap semiconductors.

Materials	Melting Point (°C)	Energy Band Gap at 300 K (eV)
ZnTe	1295 [7]	2.28 [8]
CdS	1405 [9]	2.36 [10]
ZnSe	1526 [9]	2.69 [11]
ZnS	1718 [9]	3.69 [11]

range of interest are atomic species of Group II elements, such as Zn and Cd, and diatomic molecules of Group VI elements, i.e., S_2, Se_2 and Te_2 [15–20], whereas those for IV-VI compounds under metal (Group IV) saturated conditions are the congruent subliming molecular species such as PbTe [21–23], SnTe [23–25] and GeTe [23] and the predominant vapor species for the Hg-VII_2 compounds are HgI_2 and $HgCl_2$ [26]. In the latter case, i.e. when the predominant species is the congruent subliming molecule, the transport process can be described as diffusion of the congruent subliming species from the source material through a stagnant residual gas to the deposited crystal [27]. Therefore, the transport rate is controlled mainly by the temperatures of the source and the deposition. In the former case, the partial pressures of the species II and VI_2 in equilibrium with the II-VI semiconducting compounds, at a fixed temperature, can vary by orders of magnitude as the composition of the compound varying over the narrow homogeneity range from Group II saturation to Group VI saturation [15,17,20]. As a result, the transport rate of the vapor species can also vary from a maximum transport rate corresponding to the condition of congruent sublimation, i.e., the compositions of the solid phase and the equilibrium vapor phase are the same, to transport rates which are orders of magnitude lower when the solid composition deviates significantly from the congruent sublimation. Generally speaking, in the growth temperature range usually adopted the congruent sublimation condition does exist inside the homogeneity range of these II-VI materials [17,20] but a precise control of the stoichiometry of the starting compound from the weighing of the constituent elements is practically impossible. However, with certain heat treatment methods the partial pressures over the starting compound material can be reasonably reproduced.

In Section II, a theoretical calculation of the transport rates for the II-VI compounds using a one-dimensional diffusion model will be presented and the calculated transport rates are basically determined by four parameters — the temperatures at the source and the deposition, the ratio of the partial pressures over the source and the partial pressure of the residual gas. In Section III, the experimental heat treatment methods which control the partial pressures of the starting materials will be discussed. The effectiveness of the heat treatment methods was studied by partial pressure measurements using optical absorption technique which will be the subject of Section IV. Also in section IV, the measurements on the pressure and the compositions of the residual gas by a total pressure gauge technique will be presented. In Section V, an in-situ dynamic technique for the transport rate measurements will be described and a further extension of this technique which simultaneously measures the partial pressures and the transport rate will also be included. The crystal growth experiments will be presented in Section VI which describes the furnace design, the growth parameters and the advantages of the process. A brief discussion of the characterization process, which emphasizes on the analysis of the crystalline structural defects, will be given in Section VII. The chapter will be concluded with Discussion in Section VIII.

II. Theoretical Calculation — One Dimensional Diffusion Analysis

The crystal growth of PVT consists of essentially three processes: the sublimation of the source material into vapor species, the transport of

the vapor species from the source region to the deposition region, and the condensation of the vapor species to form crystal. Under the conditions usually adopted for the PVT of II-VI compounds, vapor transport is the rate-limiting process. To improve the crystal growth rate in the physical vapor transport process, the mechanism of the vapor transport needs to be studied carefully.

Since the equilibrium vapor pressures over these II-VI compounds are relatively low (10^{-3}–10^{-1} atm) [15–20] at the usual growth temperatures, any convective contribution to the mass transport in these PVT system can be neglected. For example, in a typical ZnSe PVT growth experiment, the thermophysical properties of the growth system characterized experimentally in the following sections are listed in Table 2. Using the simplified Klosse-Ullersma model [28] and the listed properties, the ratio of the convective to the diffusive flux in a horizontal configuration is 4×10^{-10}. The process can, therefore, be well described by a one-dimensional diffusion limited analysis. The theory of diffusion in ideal multispecies gases was developed about a century ago mainly by Maxwell and Stefan. The original form of a Maxwell equation for diffusion of species A through species B was

$$-dP_A = \alpha_{AB}\frac{\rho_A\rho_B}{M_AM_B}(u_A - u_B)\,dy,$$

where P_A is the partial pressure of A along the distance y, ρ's the partial densities, M's the molecular weights, u's the velocities of the species in the direction of net diffusion, and α_{AB} a proportionality constant. Conventionally, the mass flux, or the rate of diffusion of the species A in moles per unit time per unit area, $J_A=u_A\rho_A/M_A$ is used and for a multispecies system we have Maxwell equations of the form

$$-\frac{dP_i}{dy} = \sum_{j\neq i} r_{ij}(J_iP_j - J_jP_i), \quad i = A, B, \ldots \quad (1)$$

where $r_{ij}= \alpha_{ij}/RT=RT/D_{ij}P$, $r_{ij}=r_{ji}$, and D_{ij} is the binary diffusion coefficients. Eq. (1) is accurate only when the temperature, T, and total pressure, P, are constant throughout the volume in which the diffusion takes place.

Table 2. Thermophysical properties of a ZnSe PVT growth system.

T(source)	1160°C
T(crystal)	1130°C
P_{Zn}	0.011 atm
P_{Se_2}	0.0007 atm
$P_{residual\ gas}$ (36% CO_2, 26% CO, 26% N_2 and 12% H_2)	0.01 atm
β (thermal expansion) = 1/T	7.1×10^{-4} K^{-1}
ρ (density)	1.2×10^{-5} g/cm^3
η (viscosity)	4.3×10^{-4} poise
μ (kinematic viscosity) = η/ρ	36 stoke
a (radius)	0.75 cm
L (length)	10 cm
g (gravitational acceleration)	980 cm/s^2

For the PVT growth process of a wide band gap II-VI compound, the total pressure maintains constant throughout the ampoule because of a extremely short mean-free-path of the molecules. The temperature difference commonly experienced between the source material and the grown crystal, 10 to 20°C, is small compared to the absolute temperatures used for the process. Therefore, Eq. (1) has been used satisfactorily to describe the mass transport of these systems.

When in equilibrium, the metal component forms only monomers while the chalcogens are dominated by dimers in the vapor phase. All the other thermodynamically possible chalcogen

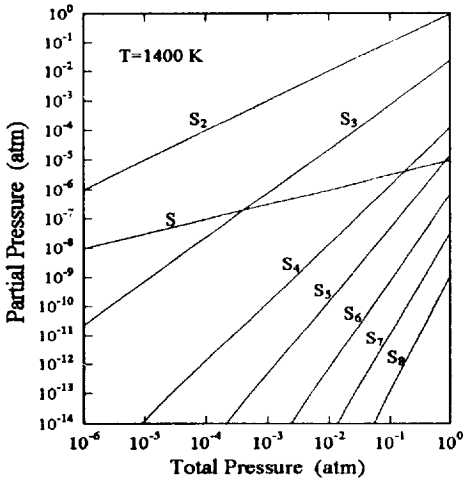

Figure 1. Partial pressures of various sulfur species as a function of total pressure at 1400 K.

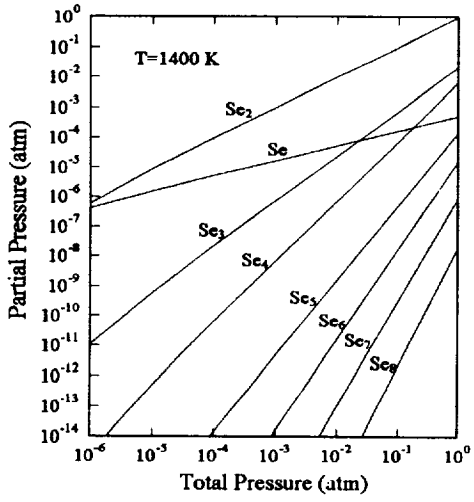

Figure 2. Partial pressures of various selenium species as a function of total pressure at 1400 K.

monomers or polymers have partial pressures at least 2 orders of magnitude lower than that of the corresponding dimers, as illustrated in Figures 1, 2, and 3, for S, Se, and Te, respectively. Therefore, only metal monomer and chalcogen dimer need to be considered in the analysis. Another interesting thermodynamic property for the II-VI compounds is that the Gibbs free energy of formation for the vapor phase is, within experimental error, independent of the deviation from stoichiometry and a function of temperature only. Table 3 lists the parameters of the equilibrium constant K(T) for the various systems.

1. Binary Case.

In a PVT process, a binary compound $A^{II}B^{VI}$ sublimes dissociatively according to the following reaction:

$$AB\,(s) \rightarrow A\,(g) + \frac{1}{2}B_2\,(g)\,. \qquad (2)$$

Two Maxwell equations need to be solved. A correlation between two fluxes has to be assumed in order to solve them since only one of the equations is independent due to the constant total-pressure condition. Obviously, $J=J_A=2J_B$ ($B \equiv B_2$ in subscript) is justified because of the fact that all the II–VI compounds have very narrow homogeneity range and no secondary phase was observed in the grown crystals. Using this and

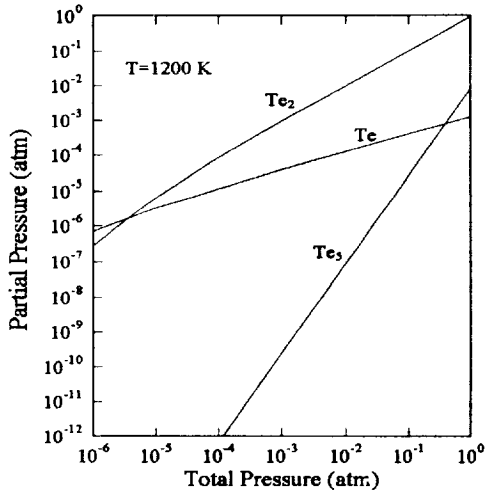

Figure 3. Partial pressures of dominant tellurium species as a function of total pressure at 1200 K.

Table 3. Parameters for equilibrium constants of various $A^{II}B^{VI}$ compounds.

$$\log P_A P_{B_2}^{1/2}\,(\text{atm}) = -C/T + D$$

Compounds	C (K)	D	Ref.
ZnS	19942	10.264	[15]
ZnSe	17818	9.1888	[16]
ZnTe	16350	9.680	[17]
CdS	17247	10.466	[18]
CdSe	16632	10.092	[19]
CdTe	15003	9.8224	[20]

$P = P_A + P_B$, the two Maxwell equations can be decoupled and reduced to

$$J = \frac{3}{2}\frac{J}{P}P_A - \frac{1}{r_{AB}P}\frac{dP_A}{dy}, \tag{3}$$

$$J = 3\frac{J}{P}P_B - \frac{2}{r_{AB}P}\frac{dP_B}{dy}, \tag{4}$$

respectively. Eqs. (3) and (4) are equivalent to those derived by Faktor and Garrett [29], where the first term on the right-hand side is called the Stefan flow term. The integration of Eqs. (3) and (4) leads to

$$P_A(y) = \frac{2}{3}P + \left[P_A(L) - \frac{2}{3}P\right] \times \exp\left[\frac{3}{2}Jr_{AB}(L-y)\right], \tag{5}$$

$$P_B(y) = \frac{1}{3}P + \left[P_B(L) - \frac{1}{3}P\right] \times \exp\left[\frac{3}{2}Jr_{AB}(L-y)\right]; \tag{6}$$

and

$$J = \frac{2}{3}\frac{D_{AB}P}{RTL}\ln\frac{P_A(0) - \frac{2}{3}P}{P_A(L) - \frac{2}{3}P} = \frac{2}{3}\frac{D_{AB}P}{RTL}\ln\frac{P_B(0) - \frac{1}{3}P}{P_B(L) - \frac{1}{3}P}, \tag{7}$$

in which y=L is where the source is located, 0 is where the crystal is, and J is positive (In Eqs. (1), (3), and (4), the flux is defined as positive in the positive y-direction. When considering a transport from L to 0 the flux becomes negative. However, we still use a positive J here by having adjusted the signs in Eqs. (5)–(7)). Eq. (7) has been used by Su [30] and Sha et al. [16] to analyze the CdS and ZnSe system, respectively. Figure 4 shows the results calculated from Eq. (7) for the mass flux in ZnSe system as a function of $\Delta T \equiv T(L)-T(0)$ for different stoichiometries of the source. The binary diffusion coefficients were computed from the Chapman-Enskog formula using the collision integral given by Neufield et al. [31]. The molecular parameters used for the computation are given in Table 4. From Eq. (7), one can find that when $P_A=(2/3)P$, or equivalently $\alpha(L)\equiv P_A(L)/P_B(L)=2$, the flux J is infinite, in which case, the mass transport is no longer limited by diffusion or by stoichiometric excess. This condition was also quoted in literature as P_{min} because it corresponds to a minimum in the total pressure. A good discussion on this was given in Ref. [29].

In a real PVT process, however, volatile impurities such as H_2, H_2O, CO, CO_2, N_2, and O_2 may be present resulting from the outgassing of the silica ampoule and/or from source material [36] and form a significant amount of residual gas. Systematic studies have been reported [37–39] on the residual gas formation in sealed silica ampoules. Since these residual species remain in the vapor phase, a third, stagnant component should be included in the diffusion analysis. Faktor and Garrett [29] gave an approximate treatment similar to the one for the two-species problem, which is valid only when the stagnant component is dominant and all three binary diffusion coefficients are equal. The analytical solu-

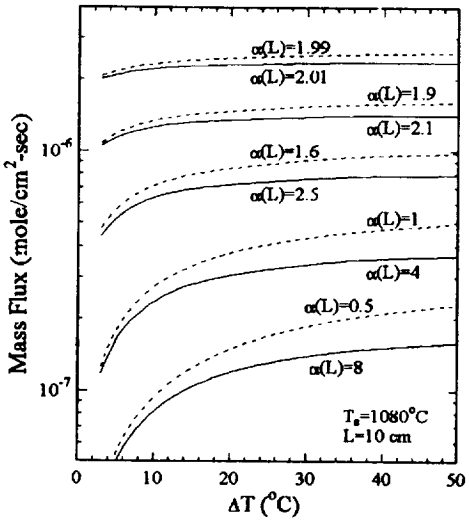

Figure 4. Calculated mass flux of ZnSe as a function of ΔT for source temperature at 1080°C and different values of α(L). Solid lines are for α(L)>2 and dashed lines for α(L)<2.

Table 4. Molecular parameters used for computing binary diffusion coefficients.

Species	σ (Å)	ε/k (K)	Ref.
Zn(g)	4.70	522	[32]
Cd(g)	4.10	557	[32]
S_2(g)	3.97	1183	[33]
Se_2(g)	3.576[a]	1130[b]	
Te_2(g)	3.887[a]	1490[b]	
CO(g)	3.690	91.7	[34]
CO_2(g)	3.941	195.2	[34]
N_2(g)	3.798	71.4	[34]
H_2(g)	2.827	59.7	[34]

a. Estimated from the molar volume at the melting point [34,35].
b. Estimated from the normal boiling temperature [31,34].

tions to the Maxwell equations for a three-species problem were first given by Gilliland [40] and can be derived in the following way:

The third equation can be decoupled by setting J_Z=0 with Z standing for the residual gas component which represents all the residual species in the vapor phase other than the two transport species (A and B_2) and whose molecular parameters can be calculated as weighted averages based on the composition of the residual gas. We have

$$\frac{dP_Z}{dy} = (r_{AZ}J_A + r_{BZ}J_B)P_Z. \qquad (8)$$

Integration yields (for transport from L to 0)

$$\ln\frac{P_Z(y)}{P_Z(L)} = (r_{AZ}J_A + r_{BZ}J_B)(L-y). \qquad (9)$$

Using $P_Z = P - P_A - P_B$ in the first two equations, we get

$$\frac{dP_A}{dy} = (r_{AB} - r_{AZ})J_A P_B - (r_{AB}J_B + r_{AZ}J_A)P_A + r_{AZ}J_A P = a_1P_A + b_1P_B + c_1, \qquad (10)$$

and

$$\frac{dP_B}{dy} = (r_{AB} - r_{BZ})J_B P_A - (r_{AB}J_A + r_{BZ}J_B)P_B + r_{BZ}J_B P = a_2P_A + b_2P_B + c_2. \qquad (11)$$

A linear combination of Eqs. (10) and (11) needs to be sought such that the ratio of coefficient of P_B to that of P_A is the same for both sides, and then, a new variable will be introduced before integration is performed. Namely, we need to construct $\beta_1\times(10)+\beta_2\times(11)$ with β_1 and β_2 satisfying

$$\frac{\beta_2}{\beta_1} = \frac{b_1\beta_1 + b_2\beta_2}{a_1\beta_1 + a_2\beta_2}. \qquad (12)$$

Let β_1=1, we find

$$\beta_2 = -\frac{r_{AB} - r_{AZ}}{r_{AB} - r_{BZ}} \frac{J_A}{J_B}. \quad (13)$$

Using Eq. (12) and proper expressions of a's, b's, and c's, we can write

$$\frac{dP_A}{dy} + \beta_2 \frac{dP_B}{dy} = -r_{AB}(J_A + J_B) \times (P_A + \beta_2 P_B + \beta_3), \quad (14)$$

where

$$\beta_3 = \frac{c_1 + c_2\beta_2}{a_1 + a_2\beta_2} = -\frac{r_{AZ} - r_{BZ}}{r_{AB} - r_{BZ}} \frac{J_A}{J_A + J_B} P. \quad (15)$$

Introducing a new variable $\bar{P} = P_A + \beta_2 P_B + \beta_3$ and integrating over it yields

$$\ln \frac{\bar{P}(y)}{\bar{P}(L)} = r_{AB}(J_A + J_B)(L - y). \quad (16)$$

Combining Eqs. (13), (15), and $r_{ij}=RT/D_{ij}P$, we can rewrite Eqs. (9) and (16) as

$$\frac{J_A}{D_{AZ}} + \frac{J_B}{D_{BZ}} = \frac{P}{RT(L-y)} \ln \frac{P_Z(y)}{P_Z(L)}, \quad (17)$$

$$\frac{J_A + J_B}{D_{AB}} = \frac{P}{RT(L-y)} \times \ln \{ [(1 + J_B/J_A) P_A(y) - a(1 + J_A/J_B) P_B(y) - b] \times [(1 + J_B/J_A) P_A(L) - a(1 + J_A/J_B) P_B(L) - b]^{-1} \}, \quad (18)$$

where

$$a = \frac{r_{AB} - r_{AZ}}{r_{AB} - r_{BZ}}, \quad b = \frac{r_{AZ} - r_{BZ}}{r_{AB} - r_{BZ}} P. \quad (19)$$

Again, $J=J_A=2J_B$ should be used in the calculation. Eqs. (18) and (19) have been used by Sha et al. [16] and Palosz et al. [41] to analyze the mass transport in the PVT systems of ZnSe and CdTe, respectively.

For the given values of T(L), T(0), and $\alpha(L)$, $P_A(L)$ and $P_B(L)$ are calculated from the equilibrium condition $P_A(L)P_B^{1/2}(L) = K(T(L))$. Then $P_A(0)$, $P_B(0)$, $P_Z(0)$, and the mass flux J can be solved from Eqs. (17) and (18) with y=0, $P_A(0)P_B^{1/2}(0) = K(T(0))$, and the constant total-pressure condition with an input value of $P_Z(L)$. The second step can be repeated for different $P_Z(L)$ until the average residual pressure, $\overline{P_Z} = (1/L)\int_0^L P_Z(y)\,dy$, matches the experimentally determined pressure of the residual gas.

Figure 5 shows the results calculated for the mass flux in the ZnSe-residual gas system as a function of ΔT. The residual pressure used, 0.008 atm, was a typical value measured by a total pressure gauge technique described later. Figure 6 shows the mass flux as a function of total residual gas pressure for different stoichiometries of the source. The curves in Figure 6 indicate that the residual gas starts to measurably reduce the mass flux when its total pressure approaches the excess

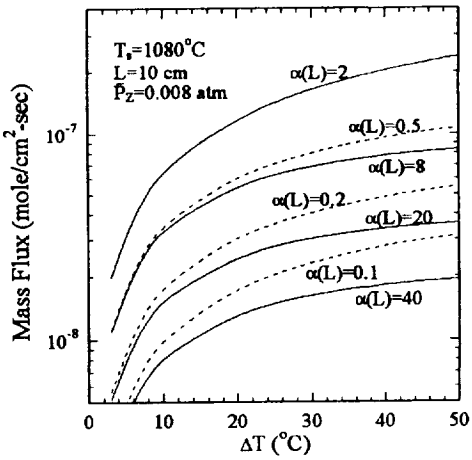

Figure 5. Calculated mass flux of ZnSe as a function of ΔT under the same condition as those in Figure 4 except a residual gas pressure of 0.008 atm is present in the system. The composition of the residual gas used in the calculation is 36% CO_2, 26% each for CO and N_2, and 12% H_2.

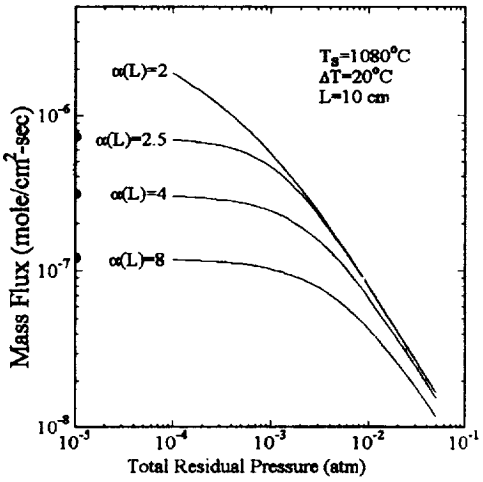

Figure 6. Calculated mass flux of ZnSe as a function of $P_Z(L)$ for source temperature at 1080°C and different values of α(L). The solid dots on the left axis are those under the same conditions but with a zero residual gas pressure.

pressure $|P_A-2P_B|$. Beyond this region, the residual gas becomes the rate-limiting factor and the α(L)-dependence of the flux becomes weak.

2. Ternary Case.

When two II-VI compounds form a ternary solid solution, such as $A^{II}B^{VI}_{1-x}C^{VI}_x$ or $A^{II}_{1-x}B^{II}_xC^{VI}$, the vapor phase contains three transport species governed by the two reactions with the proper ratio (1-x)/x. In the first case above, they are

$$AB(s) \rightarrow A(g) + \frac{1}{2}B_2(g), \qquad (20)$$

$$AC(s) \rightarrow A(g) + \frac{1}{2}C_2(g). \qquad (21)$$

If the residual gas is considered as the fourth, stagnant component, one has four Maxwell equations to solve. The fourth one can still be decoupled and integrated using $J_Z=0$ and we have an equation similar to Eq. (17)

$$\frac{J_A}{D_{AZ}} + \frac{J_B}{D_{BZ}} + \frac{J_C}{D_{CZ}} = \frac{P}{RT(L-y)} \ln \frac{P_Z(y)}{P_Z(L)}. \qquad (22)$$

The other three equations, unfortunately, cannot be solved practically to give three algebraic equations. Therefore, numerical method has to be adopted. Using the argument similar to that in a binary case a relation among the individual flux can be established, which is

$$J_A = 2(J_B + J_C) \quad \text{or} \quad J_A + J_B = 2J_C, \qquad (23)$$

depending upon the combination of the compound. If the grown crystal has only one phase, its composition can be significantly different from that of the source and should be given by

$$x(0) = \frac{J_C}{J_B + J_C} \qquad (24)$$

in the first case. From reactions (20) and (21), we have

$$\frac{P_A P_B^{1/2}}{(1-x)\Gamma_{AB}(T)} = K_{AB}(T) \qquad (25)$$

and

$$\frac{P_A P_C^{1/2}}{x\Gamma_{AC}(T)} = K_{AC}(T), \qquad (26)$$

respectively, where $\Gamma_i(T)$ is the activity coefficient of the binary compound, i, in the ternary solid solution. To perform the calculation, T(L), T(0), $P_Z(L)$, and a relation describing the stoichiometry of the source material (such as $P_A(L)/P_B(L)$ or $P_A(L)/(P_B(L)+P_C(L))$) have to be given. With the relation given above, Eqs. (25) and (26), $P_A(L)$, $P_B(L)$, and $P_C(L)$ can be calculated. Then three Maxwell equations, Eqs. (22)–(26) are used simultaneously to solve J_A, J_B, J_C, $P_A(0)$, $P_B(0)$, $P_C(0)$, $P_Z(0)$, and x(0).

Without any information on the thermodynamic properties of the ternary systems studied

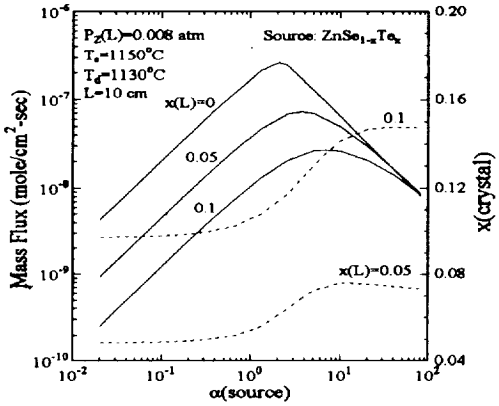

Figure 7. Calculated mass flux of $ZnSe_{1-x}Te_x$ for x=0, 0.05, 0.1 (solid curves) and the calculated compositions of the grown crystal, x(0), for x(L) =0.05 and 0.1 (dashed curves, scale on the right axis) as a function of α(L).

here, an ideal solution was assumed for these ternary solid solutions, i.e. Γ(T)=1. The mass flux and the grown crystal composition in the ternary systems were then calculated using the above procedure for the following systems:

a). $ZnSe_{1-x}Te_x$. Figure 7 shows the calculated mass flux as a function of $\alpha \equiv P_{Zn}(L)/P_{Se_2}(L)$ under the conditions of T(L)=1150°C, T(0)=1130°C, and P_Z(L)=0.008 atm for $ZnSe_{1-x}Te_x$ source materials of x=0, 0.05, and 0.1. The calculated compositions of the grown crystal, x(0), are also shown in the figure. There are three noteworthy points. (1) The mass fluxes decrease when ZnTe is introduced into the ZnSe system, (2) the maximum mass flux in the ternary system does not necessarily occur at α(L)=2.0, and (3) the composition of the grown crystal is not always equal to that, and depends strongly on the α-values, of the source material — for the case of x(L)=0.1, the grown crystal composition x(0) varies from 0.147 to 0.105 when α varies from 15 to 1. Since the partial pressure of Se_2 is the lowest in this region, which causes a lower selenium flux, and consequently, the x(0) is greater than x(L). Figure 8 illustrates the calculated mass flux of a $ZnSe_{0.9}Te_{0.1}$ source versus ΔT for various α-values near the maximum flux region. Figure 9 displays the partial pressure profiles of each species in the system along the ampoule position. It is interesting to note that, in order to maintain a constant total pressure throughout the ampoule and

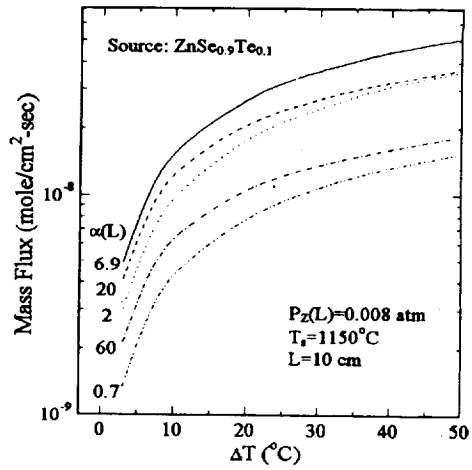

Figure 8. Calculated mass flux of a $ZnSe_{0.9}Te_{0.1}$ source as a function of ΔT for different values of α(L) near the maximum flux region.

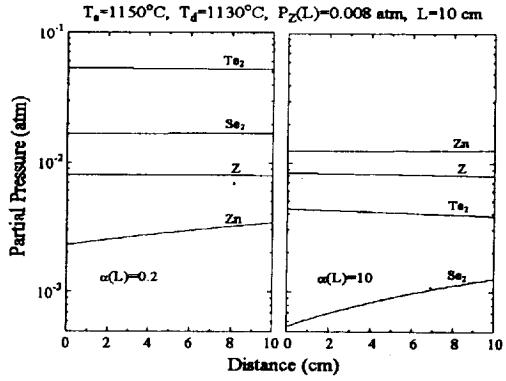

Figure 9. Calculated partial pressures of individual species along the distance of the ampoule for a $ZnSe_{0.95}Te_{0.05}$ source.

the relation among the individual flux, the tellurium and the residual species are always in a backward diffusion mode.

b). $ZnSe_{1-x}S_x$. The similar calculations were performed for the ternary $ZnSe_{1-x}S_x$ and the results are shown in Figure 10. Observations similar to the ZnSeTe case can be made with variations such as the opposite dependence of the composition of the grown crystal on the α-value. This variation is caused by the fact that the partial pressure of S_2 in this case is much smaller than that of Se_2, whereas in the $ZnSe_{1-x}Te_x$ system the partial pressure of Te_2 is always greater than that of Se_2.

c). $Zn_{1-x}Cd_xSe$. Calculations for the second example, $A^{II}_{1-x}B^{II}_xC^{VI}$, can be performed in a similar manner with the following dissociative reactions:

$$AC(s) \rightarrow A(g) + \frac{1}{2}C_2(g), \qquad (27)$$

$$BC(s) \rightarrow B(g) + \frac{1}{2}C_2(g). \qquad (28)$$

The calculated results for $Zn_{1-x}Cd_xSe$ are plotted in Figure 11 and exhibit similar features as the two cases discussed above.

The above calculations allow one to adjust

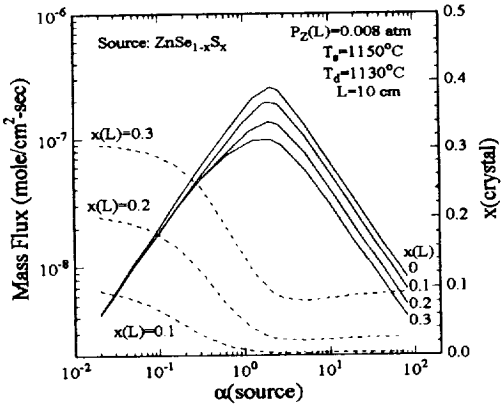

Figure 10. Calculated results for $ZnSe_{1-x}S_x$ similar to those shown in Figure 7.

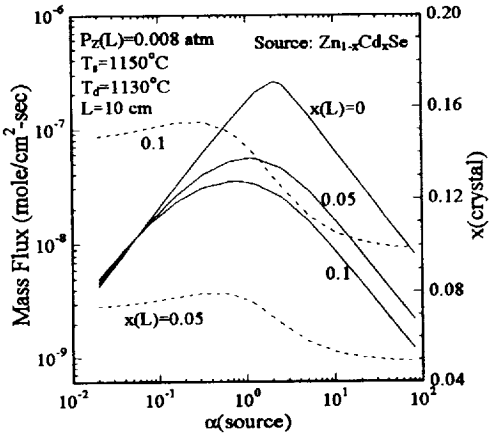

Figure 11. Calculated results for $Zn_{1-x}Cd_xSe$ similar to those shown in Figure 7.

the stoichiometry of the source to achieve a reasonable mass flux and the targeted crystal composition prior to the experiments. Palosz et al. have performed a similar calculation recently for the $Cd_{1-x}Zn_xTe$ PVT system [42].

III. Heat Treatments of Starting Materials

The calculation of last section clearly indicates that the vapor transport rate for a binary system is at its maximum when the source material sublimes congruently, i.e., the vapor phase has the same composition as the solid phase. Since the vapor partial pressures coexisting with the solid phase depends strongly on the deviation from stoichiometry of the solid, it is practically impossible to synthesize the starting material with the desired values of partial pressures by weighing of the constituent elements. One method to adjust the stoichiometry of the starting material is to bake out the material at the processing temperature under dynamic vacuum condition (method A). Besides purifying the material by preferentially subliming moisture and other volatile impurities, the process changes the stoichiometry of the starting material until the material sublimes congruently. The disadvantages of the method is the loss of the mate-

rial at a relatively rapid rate thus the temperature and the duration of the baking process has to be optimized. The other method is, after the application of method A, to distill the material by subliming it from one end of the ampoule to the other under dynamic vacuum (method B). In this case, an auxiliary heater is used to confine the deposition to a designated narrow region. In the past, these methods have been used extensively. Piper and Polich [43] baked their CdS starting material under vacuum condition and then annealed it under a stream of H_2S gas. Catano and Kun [44] removed excess Zn in their ZnSe starting material by annealing it under a flow of 1% H_2Se and 99% H_2 and then baked the ZnSe under vacuum. Kaldis [45] reduced his ZnSe starting material by baking it in dry H_2 atmosphere. Ohno et al. [46] heat treated the ZnS starting material by baking it 850°C under vacuum for 12 h then in H_2S atmosphere at the same temperature for 4 h. Burr and Woods [47] essentially heat treated their ZnSe starting materials by method B.

The heat treatment of baking under dynamic vacuum for a binary compound, in principle, only results in the congruent sublimation condition, i.e. α=2.0. To prepare a binary material with α other than 2, a two-zone annealing technique can be adopted. In this setup, the starting material at one temperature is in equilibrium with a predetermined vapor pressure of one of the elements provided by a reservoir at another temperature. Because of the stoichiometric invariant, $RT\ln P_A P_{B_2}^{1/2} = \mu_{AB}(T)$, the system variables are fixed once the temperature and one of the partial pressure are known. The technique can be extended to control the stoichiometry during the transport rate or crystal growth experiment using an in-situ heat treatment of the materials by controlling the partial pressure of one of the constituent element in the growth system. Usually, a three-zone furnace setup is employed where the temperatures of the source, the crystal (deposit) and the reservoir for the element are independently controlled. Prior [48] studied the seedless crystal growth of PbSe under controlled pressures of selenium. The group at Tohoku University, Japan, has investigated the effects of controlled over pressures on the transport rate and crystal growth of CdTe [49-52] and ZnSe [53]. Hoschl and Konak [54] grew crystals of CdTe and CdSe under controlled vapor pressures of one of the components. The group at University of Durham, England, has also studied the crystal growth of ZnSe [47,55], and CdS [56] under a controlled pressure of one of the constituent elements. In principle, the thermodynamic characteristics of these systems is well defined when (1) the amount of the element in the reservoir is large enough such that the chemical potential of the element remains the same as that of the pure element during the experiment and (2) the time is long enough for each step of the process so that the system is in steady state condition throughout the run.

The heat treatment of the starting material for a ternary system is also critical and more complicated than that of a binary system. Two methods were practiced. The first method is simply baking out the starting ternary material of a known composition, x, under dynamic vacuum. In general, for a ternary system the congruent sublimation composition does not necessarily exist inside the homogeneity range of the solid solution. For instance, in the system of a ternary solid solution $AB_{1-x}C_x$ there are three unknowns, namely P_A, P_{B_2}, and P_{C_2}, at a fixed temperature T. Under the condition of congruent sublimation given by the relations between the pressures, $P_A/P_{B_2} = 2/(1-x)$ and $P_A/P_{C_2} = 2/x$, the number of unknowns are therefore reduced to one. At the same time, the pressure products have to obey the following equations for the Gibbs energy of formation for the vapor phase:

$$RT\ln P_A P_{B_2}^{1/2} = \mu_{AB}(T, x), \qquad (29)$$

$$RT\ln P_A P_{C_2}^{1/2} = \mu_{AC}(T, x). \qquad (30)$$

There is, in general, no solution for one unknown to satisfy two simultaneous equations. The bake-out process will shift the composition of the start-

ing material continuously towards a value corresponding to a higher transport rate and eventually all the material will sublime. However, the situation described above are under the ideal condition that the kinetics in the solid is infinitely fast such that the solid phase always has a uniform composition and is in equilibrium with the vapor phase. Under the real situation the kinetics depends on various factors such as the size of the solid particles, the diffusion coefficient in the solid, and the surface area, etc.

The second method is to mix weighed amounts of two binary compounds of known pressure ratios, α [42]. The ternary starting material prepared by this method will have a well-defined and reproducible stoichiometry although the pressure ratios after the homogenization of the ternary system are not defined. As shown in the calculation of Section II, the composition, x, the temperature of the source, and a pressure ratio are needed to thermodynamically define the system variables. In the study of Cutter et al. [57], the growths of ZnSe and $ZnSe_{1-x}S_x$ with the Zn partial pressure in the system controlled by a Zn reservoir were performed and the thermodynamic condition of the system is well defined. Mochizuki et al. investigated the effects of $P_{ps} = P_{S_2} + P_{Se_2}$ and $P_r = P_{S_2}/P_{Se_2}$ on the transport rate and crystal growth of $CdSe_{1-x}S_x$ [58] and $ZnSe_{1-x}S_x$ [59] by introducing calculated excess amounts of Se and S elements into the system containing starting materials of predetermined compositions, x. There are two concerns in this case. First, the initial stoichiometry of the starting material was not well defined and, therefore, the stoichiometry of the system, including the starting material and the excess elements, was ill-defined. Second, in the extreme case when the amount of the starting material is small such that the amounts of the excess elements can provide the planned P_{Se_2} and P_{S_2} in the system, hence the two unknowns of the system, namely P_{Zn} and x, can be calculated from the two equations above using these two partial pressures and a fixed temperature, T. However, the composition of the system, x, will not necessarily be the same as that of the initial material.

IV. Partial Pressure Measurements

The mass flux in PVT process strongly depends on the partial pressures of the individual transport species as well as the partial pressure of the residual gas. Using the optical absorption technique, Brebrick and co-workers have reported the equilibrium partial pressure data over the systems of HgTe [60,61], HgSe [62], CdTe [20], ZnTe [17], ZnSe [16], PbTe [21,22], SnTe [24,25], PbSnTe [25], HgCdTe [63–65] and HgZnTe [66]. The basic principles for the measurements and the experimental procedure were described in detail in the references above. In brief, the T-shape cell for the optical measurement was made of fused silica. The sample beam of a double beam monochromator passed through the optical windows on the top of the T which was held at a fixed temperature and the sample was located at the bottom of the vertical leg of the T and held at one of a set of temperatures lower than the optical path temperature for measurement. The optical absorbance was measured between 1900 Å and 8000 Å and the partial pressures of individual vapor species were calculated using the data of calibration runs.

The vapor compositions over the starting materials for several CdTe and ZnSe ampoules were measured by the optical absorption technique. The effectiveness of the heat treatment by baking out under dynamic vacuum (method A) was confirmed by the partial pressure measurements as illustrated in Figure 12. Six batches of CdTe (total weights of 130 to 165 g) were synthesized from pure elements which were weighed to an accuracy of 0.1 mg to have the same number of moles of Cd and Te. The partial pressure of Te_2 at 870°C was determined for samples taken from each batch of as-synthesized material as well as samples that were baked for 8 min under dynamic vacuum at 870°C. The partial pressure ratio, $\alpha = P_{Cd}/P_{Te_2}$, was labeled next to each data point and $\alpha = 2.0$ corresponds to the condition of congruent sublimation. The values of α for the as-synthesized samples were always lower than 2, i.e. Te-

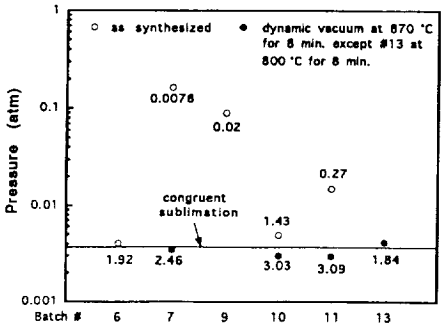

Figure 12. Partial pressure of Te_2 measured at 860°C for different batches of CdTe starting material. Open circles are the results for as-synthesized material and closed circles for the material heat treated by method A. The numbers adjacent to each data point represent the partial pressure ratio, α, and the horizontal line is the P_{Te_2} corresponding to the congruent sublimation, i.e. α=2.0, for CdTe at 860°C.

rich, and ranged from 8×10^{-3} to 1.92 whereas those for the heat treated samples ranged from 1.84 to 3.09, relatively close to 2. Measurements on three ZnSe optical cells were performed over a range of temperature. The partial pressure of Se_2 was determined from the absorbance of the Se_2 vibronic peaks at 3405, 3508, 3613, and 3792 Å and that of Zn was determined from the atomic absorption peak at 2138 Å. Because of the preferential loss of Zn to the vapor phase from the Zn-rich source and the small amounts of ZnSe materials loaded the measured α values for two of the ZnSe cells change from about 5 at 980°C to 2.7 at 1130°C. A ZnSe transport ampoule, ZST-4, was opened after the transport rate measurements (which will be discussed in Section V) and all the material was collected and loaded into an optical cell for the partial pressure measurements. The measured value for α was 38 at 1050°C. Judging from the measured transport rate of ZST-4 reported later in Section V, the source material could have an α value lower than 38 and the speculation was that it is practically impossible to collect all the material in a transport ampoule. Therefore, to have a more meaningful experiment, simultaneous measurements of the partial pressures and the transport rate were performed on a ZnSe ampoule, ZSTO-3, shown in Figure 13. The ampoule was 18 mm OD, 15 mm ID with one end tapered and an optical window configuration attached to the other end. The results of the simultaneous measurements will be presented in Section V.

The L-shape tip on the side of the ampoule in Figure 13 was fabricated for the measurement of residual gas after the transport experiment. The technique and the apparatus for the measurement was described in Ref [39]. Briefly, the processed ampoule was placed in a vacuum chamber connected to a pressure gauge and a high vacuum system. After outgassing the chamber and the ampoule for several hours at room temperature under high vacuum, the valve between the chamber and the vacuum system was closed. Then, the ampoule was slid so that the tip was struck by an obstacle and broken and the pressure change in the chamber was recorded. The original pressure in the sealed ampoule was calculated based on the chamber-to-ampoule volume ratio. Determination of the gas composition was made by selectively freeze-out of the gas components in the cold finger cooled to a predetermined temperature with appropriate cold bath mixtures. For temperatures below 77 K, the tip of the cold finger was placed in a stream of liquid helium droplets and the changes in the pressure as a function of temperature were recorded. Based on the literature [36], it has been assumed that the residual gas may consist of H_2, H_2O, CO, CO_2, N_2, and O_2 molecules. The amount of CO, N_2, and O_2 could not be determined separately by this technique. From the mass spectroscopic studies [67,68], the presence of O_2 in residual gas can be ignored. Also, the presence of H_2 in most of our ampoules precludes the simultaneous presence of O_2 at elevated temperatures. For these reasons it was assumed that the amount of O_2 in the residual gas under our experimental condition is negligible. Table 5 lists the pressures and the compositions of several ampoules after the transport process. All the start-

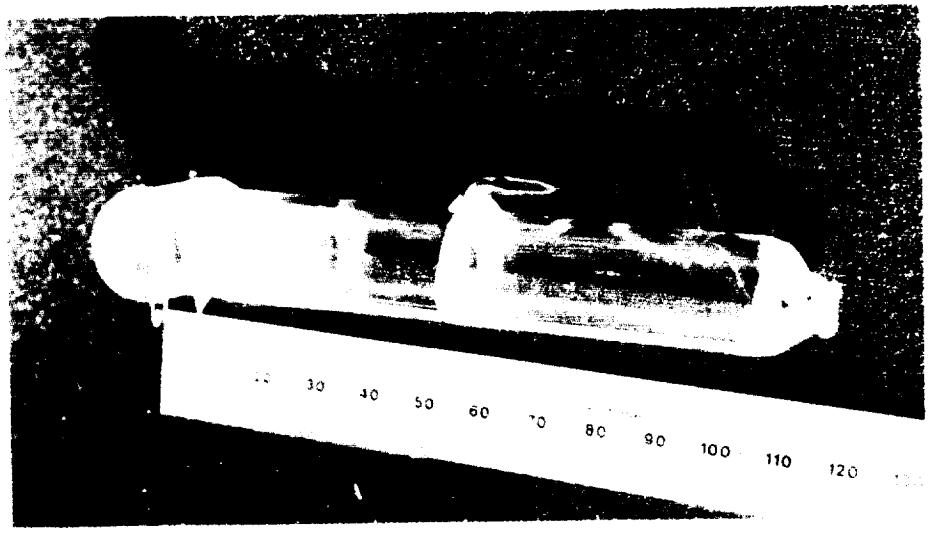

Figure 13. A ZnSe ampoule for the simultaneous measurements of partial pressure and transport rate.

Table 5. Residual gas in the growth and transport ampoules of ZnSe.

Sample	Total Pressure at Room Temperature (atm)	H_2O %	CO_2 %	$CO+N_2$ %	H_2 %
ZST-6	4.132×10^{-3}	<1	30	62	8
ZST-7	1.092×10^{-3}	<1	43	35	21
ZST-9	1.658×10^{-3}	<1	42	48	10
ZST-10	1.947×10^{-3}	<1	28	64	8
ZSTO-3	4.961×10^{-3}	2	0.2	96.5	1.3

ing materials of these ampoules were heat treated by distillation (method B) except ZST-9 which was heat treated by baking out under dynamic vacuum (method A). The majority species is CO_2 which accounts for 28–43% of the total except for the ZSTO-3 ampoule. CO and N_2, together contributed 97% in the ZSTO-3 ampoule and 35–64% in the others.

In Ref [39], empty ampoules made of silica glass from various vendors were cleaned and sealed under vacuum and the pressure and composition of the residual gas were measured after the ampoules have been heat treated by different procedures. The results show that the measured residual gas pressure was in the range of 8.6×10^{-5} to 2.3×10^{-4} atm at room temperature for three different silica brands, GE-214, ST-10 and HLQ-210, after the ampoules were outgassed at 1080°C for 16 h and annealed at 1080°C for 168 h. The silica tubing used for those ampoules listed in Table 5 were GE-214 and the ampoules were outgassed at 1060°C for 16 h before a process of the transport

rate measurements typically at 1100°C for 7 days. The comparison of the residual gas pressures between the ZnSe processed ampoules and those ampoules heat treated under similar conditions but without the presence of ZnSe indicates that the total residual pressures in the ZnSe ampoules are about one order of magnitude or more higher. The facts that the gas composition of the ZnSe ampoules is dominated by carbon oxides (CO and CO_2) whereas that of the empty ampoules consists mainly of hydrogen and water [39] implies that the ZnSe starting material was the potential source of carbon and oxygen in these processed ZnSe ampoules.

V. Transport Rate Measurements

Measurements on vapor transport rate have been reported using various technique which can be classified into two categories: (1) visual observation of the linear growth velocity of the deposition in a sealed ampoule inside a transparent furnace for systems such as HgI_2 [69,70], CdTe and PbTe [71] and (2) measurements of the total change in the mass of the source (or the deposition) in a closed ampoule after the transport process has been conducted for a period of time for systems such as the chemical vapor transport of GeSe-GeI_2 [72], the PVT of CdTe [41] and those referred in Section III on the investigation of the effects of controlled over pressures on the transport rate of CdTe [49–52], ZnSe [53], $CdSe_{1-x}S_x$ [58] and $ZnSe_{1-x}S_x$ [59]. The growth temperatures for the materials discussed here are too high to be processed in a transparent furnace which utilizes a gold-plated tubular silica liner to back-reflect the infrared radiation and usually provides a maximum temperature of 900 to 950°C. The disadvantages of the second technique above are: (1) it yields the average transport rates and (2) the limitation of determining only one data point, i.e. mass flux for a fixed set of T(source) and T(deposit), from each ampoule. These results will not be compared with the theoretical calculation described in Section II mainly because either the stoichiometry of the starting material is not well-defined or the pressure and composition of the residual gas in these cases are not known. In numerous other cases, the transport condition was not well defined because either the ampoule or the furnace was translating during the growth experiments. Besides these results, some articles have also reported transport rates during their crystal growth experiments as mass transported per unit time. In these cases, the cross-section area of the growth ampoule is needed to convert the results into mass flux for comparison.

Recently, a continuous measurement of the total mass change in a closed ampoule by an in-situ dynamic technique was developed in our laboratory [16]. The experiment ampoules were made of 18 mm OD, 15 mm ID fused silica tubing and were about 12 cm in length. The cleaned and outgassed ampoule was loaded with 2 to 5 g of heat treated ZnSe and sealed at a pressure of 5×10^{-7} torr or less. A three-zone tubular resistance furnace was employed to perform the transport experiments. A schematic drawing of the setup with a typical temperature profile along the center line of an empty furnace bore are given in Figure 14. Two legs attached to the left end of the ampoule served as a fulcrum. The right end of the ampoule was connected, via a ceramic block, to a ceramic lever which extended out of the furnace and rested on a wire suspended from a Mettler AE 100 electronic balance. The temperatures, T_s at the source and T_d at the deposition, were measured by two thermocouples placed at the ends of the ampoule and together with the balance readings, were recorded by a computer at 15 or 30 min intervals. The balance readings were then converted to the mass transported using the dimensions of the ampoule/lever assembly. These data were plotted versus time and the mass flux was obtained from the slope of the curve. For most of the runs a few different temperature settings were used to determine the dependence of the mass flux on the source temperature. After all the material has transported the accuracy of the measuring system can be confirmed by comparing the total transport mass measured with the total mass

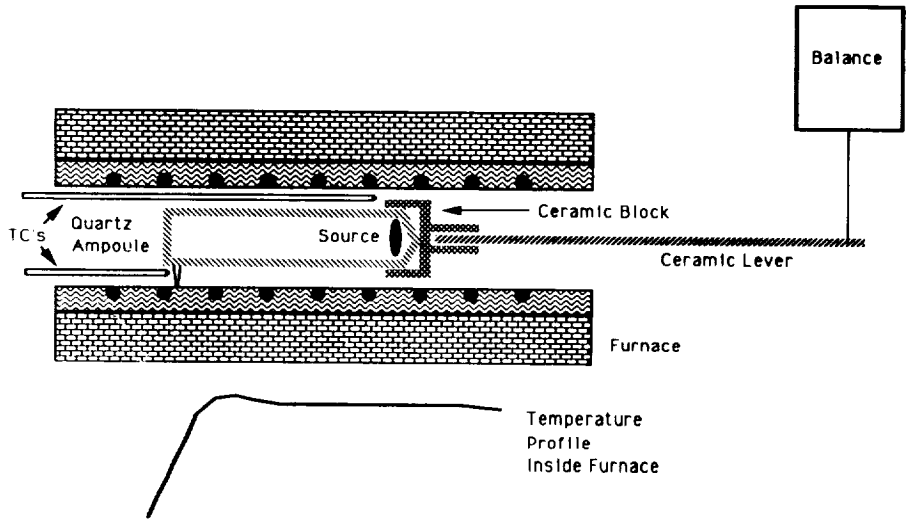

Figure 14. Schematics of the setup for the transport rate measurement by the in-situ dynamic technique.

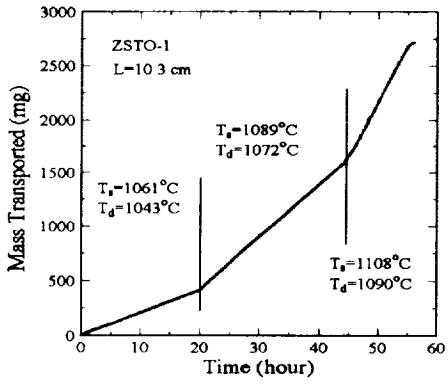

Figure 15. Measured ZnSe mass transported as a function of time for a typical run.

loaded and another run using the same ampoule can proceed by simply reversing the temperature gradient.

A series of transport experiments of ZnSe was performed using the in-situ dynamic technique. Figure 15 shows the measured mass transported as a function of time for a typical run. The results of the mass flux versus the reciprocal of the source temperature from different ampoules are plotted in Figure 16. Each mass flux value was derived from a well defined straight line generally consisting of more than 40 data points on a plot as shown in Figure 15 and was normalized to a transport length of 10 cm. With a few exceptions, the ΔT values used ranged from 13 to 20°C. The source materials from Cleveland Crystals, Inc. used for ampoules ZST-2, 4, and 5, shown as solid symbols, display in general lower fluxes with stronger temperature dependence than those of the source materials from Eagle-Picher, Inc., which were used in other ampoules and shown as open symbols. The methods of heat treatment, method A and B, as described in Section III did not show apparent effect on the measured mass transport rates.

Four parameters are needed, as discussed in Section II, to perform the theoretical calculation for a comparison with the experimentally measured transport rates. The source temperature, T(L), and the average of the pressures and compositions of the residual gas measured from the four

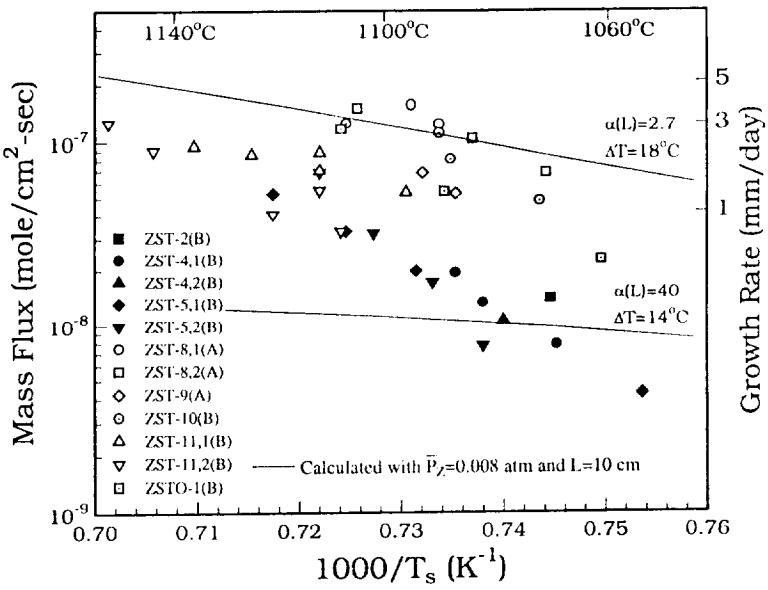

Figure 16. Mass fluxes of ZnSe as a function of reciprocal of source temperature. Solid symbols: source materials from Cleveland Crystals, Inc.; open symbols: source materials from Eagle-Picher, Inc. The letters in the parentheses in the legend indicate the method of heat treatment. The solid lines are calculated with conditions described in the text. The composition of the residual gas used in the calculation is 36% CO_2, 26% each for CO and N_2, and 12% H_2.

experiment ampoules, ZST-6, 7, 9, and 10, listed in Table 5, as given in the caption of Figure 16 were used as input values for two parameters. Two theoretical curves were calculated. The first one is the upper limit for the mass flux and it is calculated with ΔT=18°C and $\alpha(L)$=2.7 — the lowest value obtained from the partial pressure measurements over two starting materials of ZnSe as reported in Section IV. An α value of 38 was measured at 1050°C over the source material of ZST-4, also reported in Section IV. Thus, the lower limit of the mass flux was calculated using ΔT=14°C and $\alpha(L)$=40. Most of the experimental data fall between these two curves and some agree well with the upper curve which represents the highest mass flux achievable under the experimental conditions. The stronger temperature dependence of some of the measured mass flux than that of the theoretical curves could be caused by a progressive change of the source material composition toward the congruent sublimation condition as the source temperature increases.

The general agreement observed between the experimental and theoretical results of the mass flux is satisfactory. However, the actual value of α over the source, or the deposit, during the vapor transport process was not known for these measurements. In principle, this α-value can vary during the transport process because the stoichiometry of the deposit is usually different from that of the source and, therefore, the stoichiometry of the source and that of the deposit, change continuously during the transport process. To have a better understanding of the transport process, a simultaneous in-situ measurement of the transport rates and the partial pressures was designed and performed. The ampoule configuration, as

described earlier in Figure 13, is essentially the same as the transport ampoule except two optical windows were fabricated at one end for the optical absorption measurements. The short length of the optical path, 1.95 cm, was made intentionally to have an almost constant cross-section area for the mass flux throughout the length of the ampoule. The starting material of ZnSe, provided by Eagle-Picher, Inc., was heat treated by distillation under vacuum (method B). 3 g of heat treated ZnSe was loaded into an optical cell, ZSTO-3, as shown in Figure 13, and sealed under vacuum. The transport length was 10.3 cm. During the run, eight thermocouples were used to monitor the thermal field. Among these thermocouples, two of them, TC6 and TC7, provided the temperature measurements at the optical windows and the reservoir end, respectively, and the other six thermocouples were employed to insure that the material condensed only at the desired region. During the run, the material transported from the reservoir, at 1150°C, to the window end, at 1130°C, with a maximum of 1165°C in between and the partial pressures over the deposited material were measured. The optical absorbance and the balance readings were simultaneously recorded at a 30 min interval. However, during the thermocouple calibration after the transport experiments it was found that in the 1130 to 1160°C range the readings of TC7 were 10°C lower than that of TC6 when they were positioned in the same location inside the furnace. Assuming the readings of TC6 were correct, the real temperatures of the source and the deposition should be and 1160 and 1130°C, respectively. The pressure and compositions of the residual gas were measured after the experiments using the technique described in Section IV and were listed in Table 5.

The measured partial pressure of Zn and the mass transported were plotted versus time in Figure 17. The measured optical absorption of Se_2 peaks was too low, due to the combination of the low Se_2 pressure and the short optical path length used, to give accurate measurement of Se_2 pressure. Therefore, the equation for the Gibbs energy of formation listed in Table 3, together with the measured Zn partial pressures were used to calculate the partial pressures of Se_2 which were also plotted in Figure 17. The measured pressures of Zn scattered but remained almost constant throughout the run at about 0.012 atm which corresponds to a value of P_{Zn}/P_{Se_2}, α=17. The theoretical flux was calculated, using the measured parameters, i.e., thermal field, partial pressures over the deposition and the residual gas pressure, and agrees very well with the experimental data as plotted in Figure 18. The sensitivity of an error of 2°C in the T(deposit) was also given and is almost negligible. The calculated partial pressure profiles for Zn, Se_2 and the residual gas, Z, along the length of the ampoules during the run are given in Figure 19 which illustrates that both Zn and Se_2 species were in a forward diffusive mode because of the high pressure of the residual gas. The measurements of a constant partial pressure of Zn over the duration of the experiment was unexpected. It was speculated that the difference in the stoichiometry for ZnSe under the conditions of

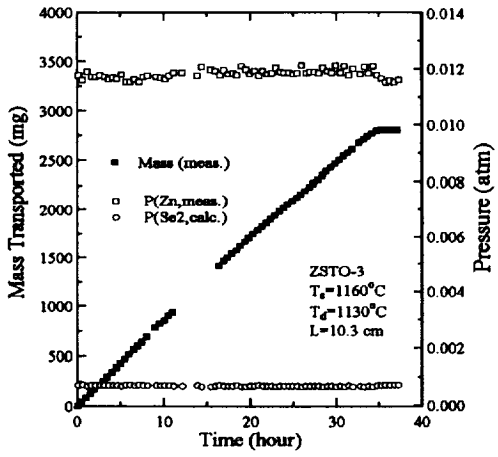

Figure 17. Measured P_{Zn} over the deposit and measured mass transported versus time for ZSTO-3. The P_{Se_2} data were calculated from P_{Zn} and the equilibrium constant.

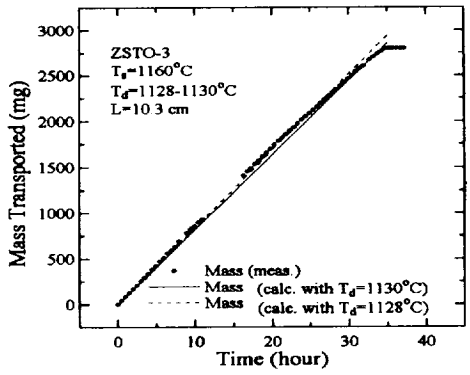

Figure 18. Comparison between the calculated and the measured mass fluxes for ZSTO-3. The measured pressure and composition of the residual gas were used in the calculation.

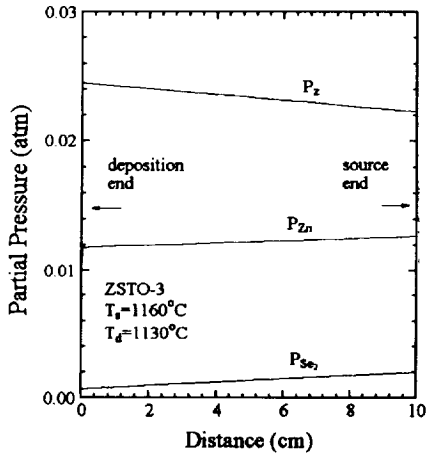

Figure 19. Calculated partial pressure profiles for Zn, Se_2, and residual gas, Z, along the ampoule length for ZSTO-3.

α(source)=6.4 at 1160°C and α(deposit)=17 at 1130°C are essentially negligible such that the stoichiometry of the ZnSe source remained the same through out the transport experiment. The excess amount of Zn in the vapor phase was also estimated. It was estimated that there were 0.12 mg of Zn and 0.036 mg of Se in the vapor and the incorporation of these amounts makes the stoichiometry of the system richer in Zn by 1.7×10^{-5} mole fraction. For the first time, the mass fluxes in a PVT system were calculated, without any adjustable parameters, by assuming a one-dimensional diffusion model and using all the input parameters measured experimentally and show good agreement with the experimental value.

In the investigation of the effects of controlled over pressures on the transport rate of CdTe [49-52] and ZnSe [53], the measured mass flux was constant when the controlled over pressure was low. When this over pressure was higher than a value in the vicinity of the partial pressure corresponding to the congruent sublimation condition the measured flux showed a dependence of P_{Cd}^{-3} (or P_{Zn}^{-3}) and $P_{Te_2}^{-3/2}$ (or $P_{Se_2}^{-3/2}$) on the controlled over pressure. These dependencies can be obtained from the exact theoretical expressions presented in Section II under the approximation that the total pressure is dominated by one vapor species. In the region where the controlled partial pressure is low, the partial pressure in the growth ampoule could not be controlled effectively by the

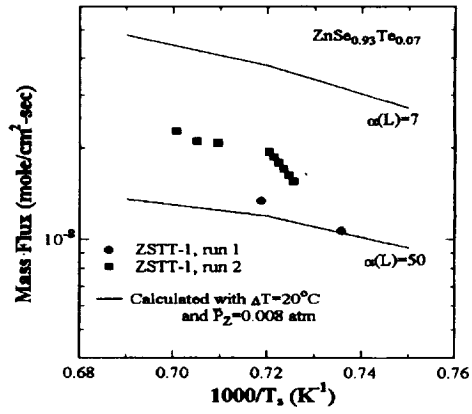

Figure 20. Measured mass flux of $ZnSe_{0.93}Te_{0.07}$ as a function of reciprocal source temperature. The solid curves are the calculated results.

reservoir chamber and the transport rate depended on the history of the source material.

A transport ampoule of the ternary system $ZnSe_{1-x}Te_x$, for x = 0.07, was prepared. 3 g of ZnSe and 0.302 g of ZnTe were loaded into the transport ampoule and sealed under vacuum. The starting material for ZnSe was previously heat treated by distillation under vacuum (method B) and that for ZnTe was treated by baking at 1000°C for 10 min under dynamic vacuum (method A). The measured mass fluxes are plotted in Figure 20 as a function of 1000/T(source). Two theoretical curves, similar to those shown in Figure 16 for the ZnSe binary system, are also plotted as the upper and lower boundaries for the experimental data. The effects of controlled over pressures on the transport rate were also studied for the system $CdSe_{1-x}S_x$ [58] and $ZnSe_{1-x}S_x$ [59]. No comparisons were made between their experimental results and our theoretical calculation because the thermodynamic condition in their experiments were not well defined as discussed in Section III.

In general, the calculation indicates that the residual gas pressure generated from the source material was the main factor that limited the transport rate. This is evidenced from the calculated results shown in Figure 21 where another set of calculated transport rates was added to Figure 16. As discussed in last Section the comparison of the residual gas pressures between the ZnSe processed ampoules and those ampoules heat treated under the similar process but without the presence of ZnSe indicates that the total pressures in the ZnSe ampoules are about one order of magnitude or more higher. The new set of results in Figure 21 was calculated using the same parameters except that typical values [39] of the residual gas pressure and composition in ampoules made of GE-214 silica glass processed without ZnSe were adopted. The calculation was supported by some preliminary transport rate measurements in our laboratory which employed a different heat treatment technique and resulted in an improvement of 4 to 6 times in the transport rate. Presumably, this was caused by a reduction in the residual gas pressure. At this time, a complete experimental and theoretical investigation is being conducted and the results will be reported in the near future.

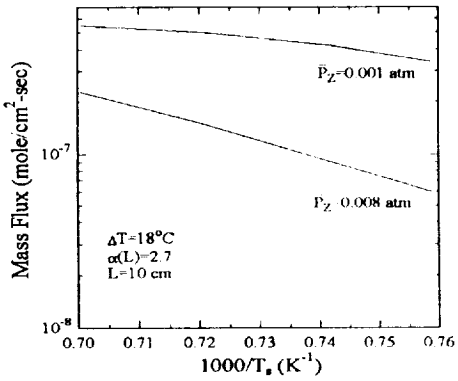

Figure 21. Calculated mass flux for ZnSe versus reciprocal source temperature. The lower curve is the same as the upper curve shown in Figure 16. The upper curve is calculated using the residual pressure and composition of those typically measured in ampoules processed without containing any material.

VI. Crystal Growth

Due to the high melting temperatures, the bulk growth of the wide band gap II-VI semiconducting compounds was mainly performed by vapor growth rather than melt growth. To increase the transport rate and consequently reduce the growth temperature the introduction of a transport agent, such as I_2, was widely employed for CdS [73], ZnSe [44,45,74–79], ZnTe [78], ZnS [46,78,79] and ZnSeS [44,79]. The disadvantage of this chemical vapor transport (CVT) technique is the high level of the unintentional doping of the transport agent [44,75,79]. On the other hand, different variations of the PVT technique have been applied. These variations include the growth in semi-open system [43,80,81] originally developed by Piper and Polich, the stationary seeded growth in a closed system for CdS [82], CdS and CdSe [83], and ZnSe [84], the translational unseeded growth in a closed system for CdS [85,86], ZnTe

[87,88], ZnSe [89–91] as well as seeded growth for CdTe [92] and the growth of CdS [56,93,94], ZnSe [47,55,57,95], ZnSeS [57,59] and CdSeS [58] under the controlled partial pressure of one (or two) of the constituent elements in a closed ampoule. It was also believed that a slow but practical transport rate improves the morphological and crystalline quality of the grown crystals [84] and, therefore, in some cases inert gas was intentionally introduced into the system [68]. The thermally induced strain and defects caused by the crucible wall was eliminated in the seeded contactless growth of CdS and CdSe reported in Ref. [82,83] and in a novel self-seeded contactless growth of CdTe [96]. The growth of doped-ZnTe by introducing small amount of In into the growth system was also reported [97].

In our laboratory, the growth activities were concentrated on the translational growth in a closed system, seeded as well as unseeded, for its experimental simplicity and minimal needs for process control in the microgravity environment of space. After the transport rate was optimized the crystal growth proceeded with the judicious choices of the growth parameters. Usually, the heat treatment technique which resulted in the highest transport rate was adopted. As shown in Figure 4, the mass fluxes are almost saturated to the maxima when $\Delta T=20°C$ for those values of α close to 2.0. Therefore, the furnace, or the ampoule, translation rate was selected to be close to but slower than the measured transport rate for a ΔT of 15 to 20°C. Both unseeded and seeded growth experiments were performed. The compositions of the vapor species in the growth ampoules can be determined by the optical absorption technique. For unseeded growth condition, this can be accomplished by using the ampoule design as shown in Figure 22(a). The material will be transported to the optical window end after the partial pressure measurements and then the crystal growth will start at the tapered end as shown in Figure 22(c). Figure 22(b) shows the ampoule design for seeded growth experiments. In the determination of the vapor pressure the procedure is the same as the unseeded condition. After the pressure measurements, the ampoule will be broken open at the neck of the optical windows and seed, quartz wool, and a quartz rod will be loaded as shown. The ampoule is then sealed under vacuum. Figure 23 shows the picture of a seeded CdTe ampoule.

Figure 22(c) also illustrates a typical temperature profile and the initial ampoule positions during a growth run [86,87]. The profile can be easily provided by a three-zone furnace with an adiabatic zone inserted between the central and the end zones. The temperature profile translates to the right during the growth. For the unseeded situation, the crystal starts to nucleate when the ampoule tip is at the supercooling position with a temperature lower than the thermal supersaturation as shown in Figure 22(c). In the case of the seeded growth, the initial ampoule position needs to be carefully adjusted such that the middle section of the seed is positioned at the supercooling position. Under such condition, part of the seed sublimes first and then the grown crystal nucleates and grows on top of the seed.

A three-zone tubular resistance furnace was used to produce a sharp gradient which resulted in a well-defined position for the supersaturated vapor phase and consequently, a well-defined solid-vapor interface. Using this method, large crystals of CdS [86], PbSe, CdTe, ZnTe [87], and ZnSe [92] as shown in Figure 24, have been grown consistently. In most of the runs, the interface of the growth crystals vary from concave (towards the crystal) for CdTe, to almost flat for ZnTe and PbSe, to slightly convex for CdS and convex for ZnSe crystals. To achieve the monocrystalline growth the precise control of the growth interface shape is critical. It is believed that a slight convex interface not only promotes favorable crystalline grain selection, eliminates the nucleation of undesirable secondary grains, also causes existing extended defects to grow towards the container wall and be eliminated, and minimizes thermally induced defects. After analyzing the thermal environment near the interface, the

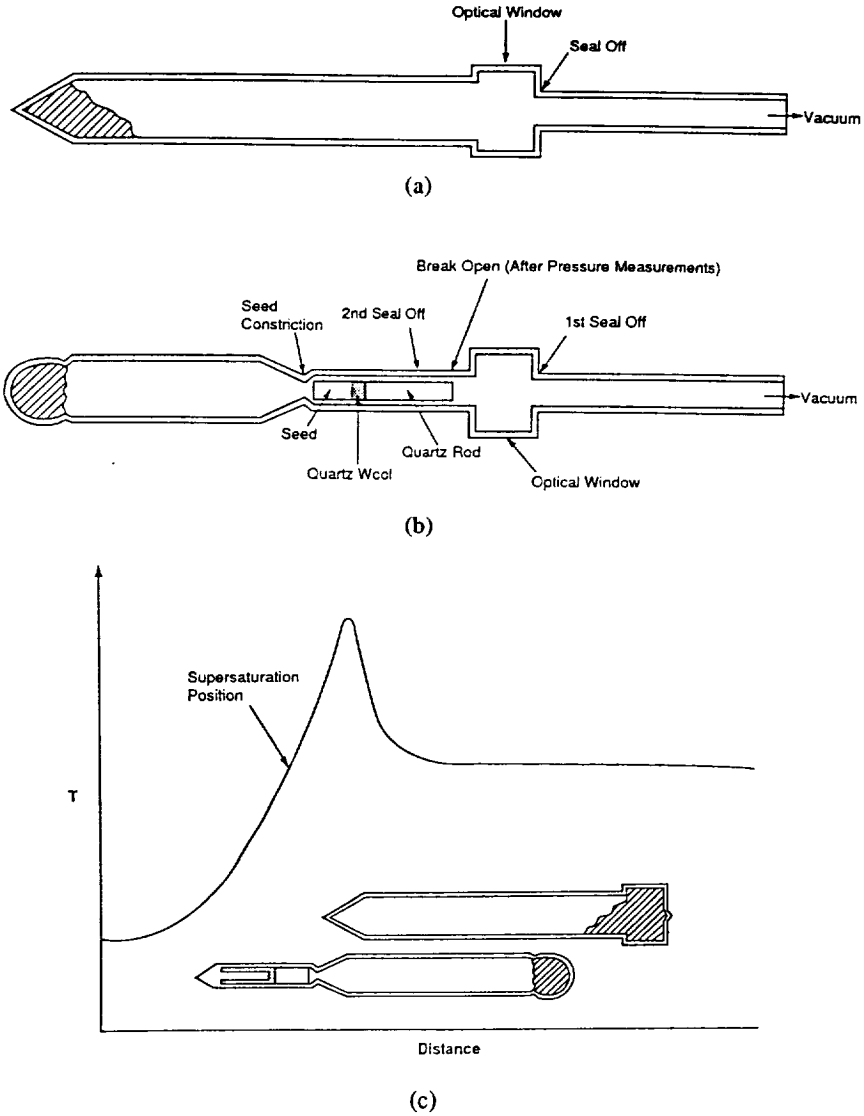

Figure 22. Schematics of the ampoules for (a) unseeded, (b) seeded growth, and (c) thermal profile and initial ampoule positions.

low thermal conductivity of the CdTe solid was considered to be the main reason for the shape of the concave interface. To modify the thermal environment an adiabatic zone (2.5 to 5 cm thick) made of ceramic form (Cotronics 310-I) was inserted between the central heater and the cold zone. This resulted in an improvement of the CdTe growth interface to a flat surface.

Figure 23. Picture of a seeded CdTe ampoule.

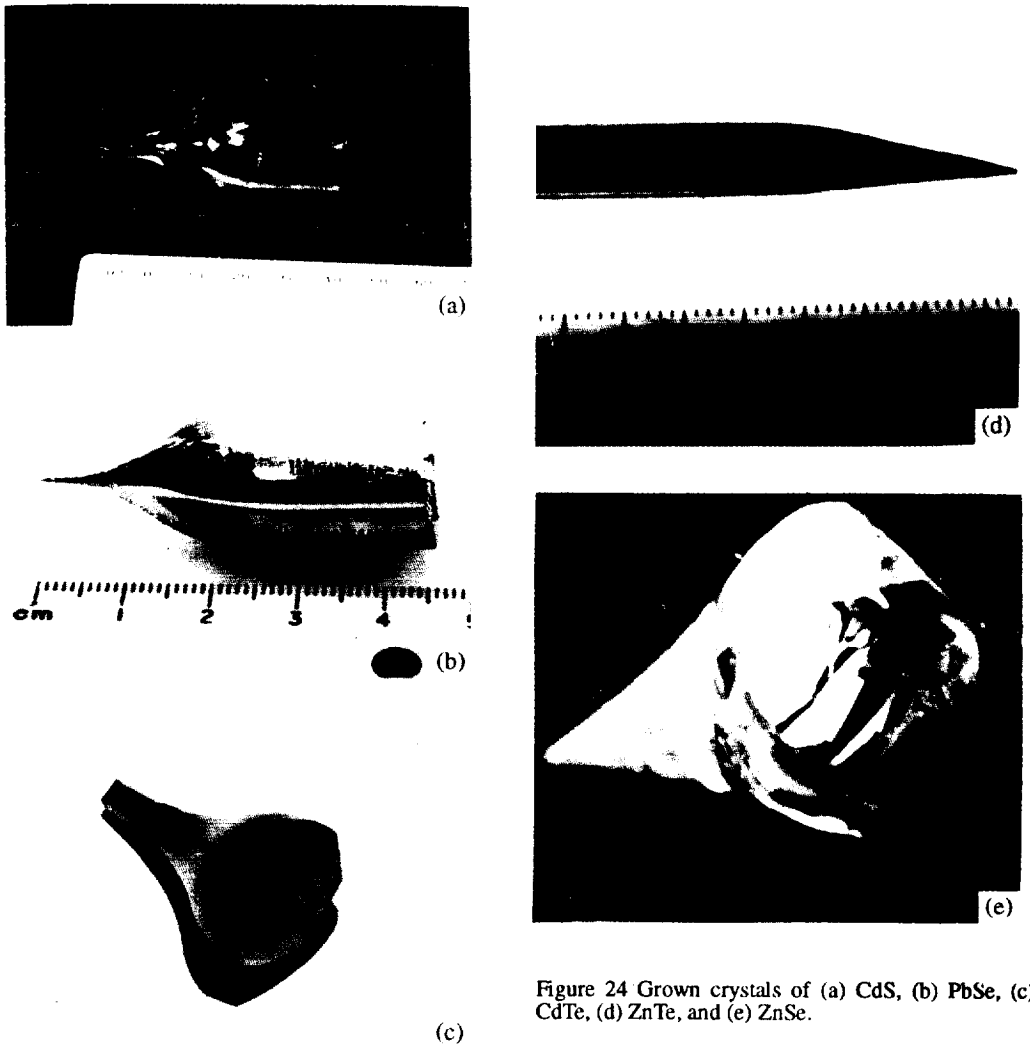

Figure 24 Grown crystals of (a) CdS, (b) PbSe, (c) CdTe, (d) ZnTe, and (e) ZnSe.

In the simple case of vapor transport experiment the onset location and the length of the deposition region depend on the temperature and partial pressure distributions along the length of the ampoule. The driving force for the growth (deposition) is the free energy change of the reaction corresponding to the vapor-solid growth process. As demonstrated in the HgZnTe-HgI_2 chemical vapor transport system [98], the location of the deposition zone can be predicted when the temperature and partial pressure profiles along the ampoule are well defined. In the growth system discussed here the degree of supercooling depends not only on the temperature and partial pressure distributions but also on the vapor transport rate of the source material and the furnace translation rate. In the simple case that the furnace remains stationary the partial pressure profiles can be calculated only when the stoichiometry, or the value of α, of the source is known. With a fixed furnace (or ampoule) translation rate one has to consider whether the degree of supercooling ΔT can provide a mass flux fast enough to keep up with the translation rate. Figure 25 shows a growth ampoule of CdS which exemplifies the case when the furnace translation rate was too fast for the vapor transport rate to maintain a stable growth interface. Table 6 illustrates the comparison between the thermal saturation position (S) — determined from the thermal profile inside an empty furnace bore and the observed growth interface position (I) for both unseeded and seeded horizontal growth of CdTe. Only those runs in which the source materials were not completely transported after the growth and similar furnace translation rates were employed are listed. Within the accuracy of measurement and the uncertainty due to the variation of the interface shape, the degree of supercooling in most of the CdTe runs were well controlled and defined. Table 7 lists the degree of supercooling in unseeded growth of ZnSe. In the case of ZnSe, the degree of supercooling was larger, as expected, for those runs with lower source temperature because in these cases a larger ΔT was needed to provide higher transport rate to keep up with the furnace translation rate. Post-growth cooling process is also critical to maintain the quality of the grown crystals. Ampoule-cracking has been observed in CdTe and ZnSe growth ampoules when the post-growth cooling rate was too high.

Figure 25. A growth ampoule of CdS with unstable growth interface.

The advantages of the temperature distribution used here for crystal growth are the following.

1. The peak in the thermal profile provides confinement of the region of supersaturation to a narrow region because of the high temperature gradient at the growth interface.

2. The peak in the thermal profile permits the position of supersaturation to be controlled independently of the transport rate which is determined by the temperature of the source material in the hot zone.

3. The peak in the profile also eliminates possible secondary nucleation sites by desorbing inadvertently deposited material from the ampoule wall just ahead of the crystal/vapor growth interface.

4. Use of furnace (or ampoule) translation assures that the position of supersaturation can and will be maintained at the growth interface throughout the growth of the entire crystal.

5. The use of the insulation (or adiabatic) zone allows for precise control of the growth

Table 6. Comparison between thermally saturated position (S) and growth interface position (I) and the degree of supercooling

I. CdTe unseeded cases

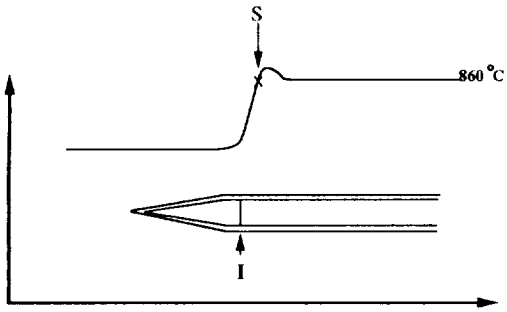

Sample	S(cm)	I(cm)	Supercooling (°C)
CdTe-7	51.2	51.15	1.9
CdTe-9	51.3	51.1	7.4
CdTe-16	49.8	49.7	3.7
CdTe-17	49.8	49.75	1.9
VCG-1	50.2	50.1	3.7
VCG-24	49.6	49.8	?

II. CdTe seeded cases

Sample	S(cm)	I(cm)	Supercooling (°C)
CdTeS-6	49.6	49.55	1.6
CdTeS-7 (I)	50.3	50.0	5.4
CdTeS-7 (II)	50.3	49.95	6.3
CdTeS-8 (I)	49.6	49.5	3.1
CdTeS-8 (II)	49.6	49.57	0.9
CdTeS-9 (I)	49.6	49.55	1.6
CdTeS-9 (II)	49.6	49.6	0
CdTeS-9 (II)	49.6	49.58	0.6
CdTeS-10 (I)	49.6	49.5	3.1
CdTeS-10 (II)	49.6	49.35	7.8
CdTeS-12 (I)	49.6	49.55	1.6
CdTeS-12 (II)	49.6	49.55	1.6
CdTeS-14 (I)	49.6	49.5	3.1
CdTeS-14 (II)	49.6	49.33	8.4
CdTeS-15 (I)	50.5	50.1	5.2
CdTeS-15 (II)	50.5	50.1	5.2

interface shape which promotes favorable crystalline grain selection, eliminates the nucleation of undesirable secondary grains, causes existing extended defects to grow toward the container wall and be eliminated, and minimizes thermally induced defects.

6. The generation of crystal defects usually results from the low yield strength at the high

Table 7. Degree of supercooling in unseeded PVT growth of ZnSe.

Sample	Source Temperature (°C)	Interface Temperature (°C)	Supercooling (°C)
ZnSe-5	1090	1065	25
ZnSe-9(#2)	1080	1057	23
ZnSe-14	1070	1050	20
ZnSe-15	1075	1045	30
ZnSe-15(#6)	1140	1135	5
ZnSe-18(#2)	1150	1138	12
ZnSe-19	1150	1138	12

growth temperatures required to achieve monocrystal growth. The yield strengths of materials in general rapidly increase with decreasing temperature. With the method and apparatus described here, growth can be accomplished at temperatures lower than commonly used. This allows the production of crystals with a higher degree of perfection because of the increased crystal yield strength.

VII. Characterization

Very extensive characterization technique on the grown crystals has been reported and will not be discussed in detail here. In general, these technique were applied to characterize the crystalline structural properties as well as the electrical and optical properties of the grown crystals. In our laboratory, the studies on the structural defects, including impurities, voids, precipitates, dislocations, slip bands, small angle grain boundaries, twins and compositional variation in ternary compounds were accomplished by various technique such as Spectroscopy (atomic absorption and spark source mass spectroscopy), X-ray diffraction (Laue reflection and rocking curve), synchro-

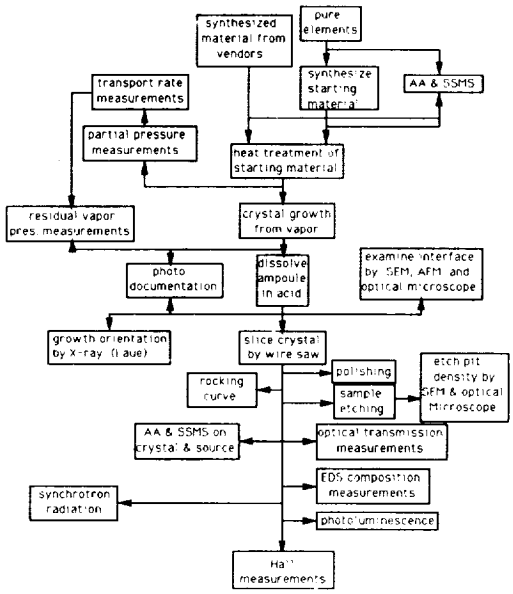

Figure 26. A flow chart of the materials preparation and characterization procedure.

tron radiation images of white X-ray beam (reflection and transmission), Microscopy (optical, electron, and atomic force), sample polishing and etching and optical transmission. The electrical and optical characterization was performed by optical transmission, photoluminescence, and Hall measurements.

Figure 26 shows the flow chart of the material preparation and characterization technique practiced in this investigation. The characterization results on the wide band gap II-VI semiconductors are reported briefly below.

1. Microscopy. Optical and electron microscopy were employed to study growth surface morphology and structural defects (after appropriate chemical etching) such as voids, precipitates, dislocations, small angle grain boundaries and twins. The ZnSe crystals cleave easily along (110) planes which are also the planes that growth facet developed. The growth steps on the growth surface of a ZnSe crystal is shown in Figure 27. Figure 28 presents pictures of typical dislocation etch pits on a CdS (0001) plane (a), a micrograph of an over etched CdS (0001) sample to delineate the hexagonal lattice structure (b), and etch pits on a ZnSe (111)B plane (c). Atomic force microscopy (AFM) provides the technique for the study of nanometer-structure on the crystal surface. The morphology of freshly cleaved (110) surfaces of ZnSe crystals was examined by AFM [99] and shown in Figure 29. The particles with the size of about 20 nm were identified by differential scanning calorimetry [99] to be Se-rich eutectic and from Figure 29 some segregation effect of the precipitates along low angle grain boundaries was evident. However, in the ZnSe crystals grown from the source materials provided by other vendor and under different thermal conditions the Se-rich precipitates were not observed [99].

2. X-ray Laue diffraction. The growth orientations of unseeded single crystals were routinely determined by X-ray Laue technique. Cutter et al. [57] reported that the growth surfaces of ZnSe crystals have tendency to be close to the (111)B (Se face) plane. Our preliminary results, as shown in Figure 30, indicate a random preference for the growth orientation.

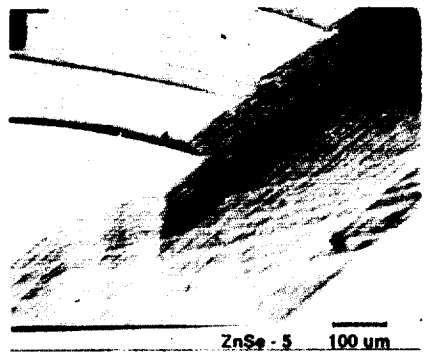

Figure 27. Growth steps on the growth surface of a ZnSe crystal.

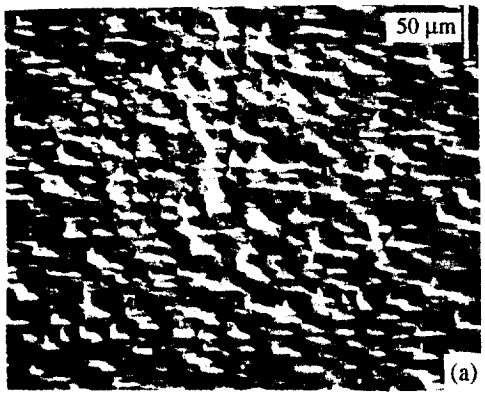

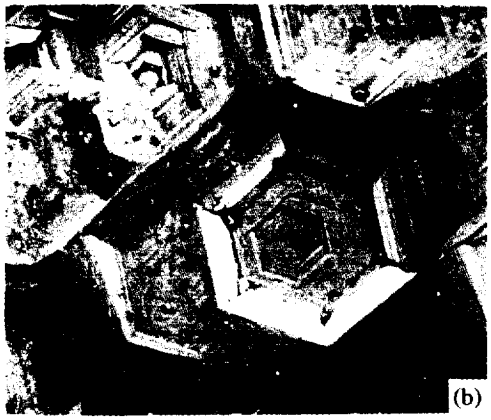

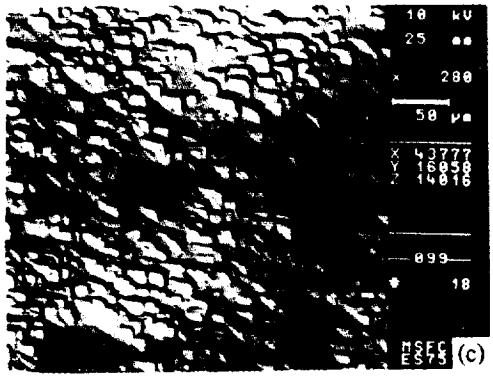

Figure 28. (a) Dislocation etch pit density of 1–2×10^4/cm^2 on a CdS (0001) plane; (b) a micrograph of the hexagonal structure of the CdS etch pits; and (c) dislocation etch pit density of 1×10^5/cm^2 on a ZnSe (111)B plane.

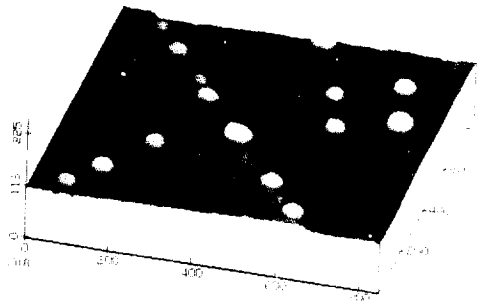

Figure 29. AFM picture of a freshly cleaved (110) surface of a ZnSe crystal with Se-rich precipitates.

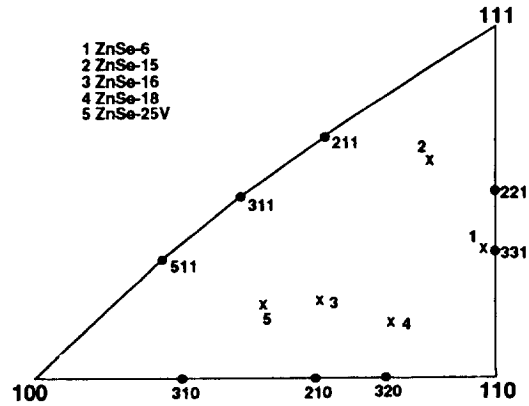

Figure 30. Growth orientations of unseeded single crystals of ZnSe. All growths are in horizontal configuration except ZnSe-25V is in vertical stabilized configuration.

3. Optical absorption. The room temperature measurement of optical absorption (or transmission) spectra is a convenient yet accurate method for the compositional mapping of a ternary semiconducting wafer [100]. The low temperature (4.2 K) infrared absorption measurements was used to detect the impurity absorption in the crystal

[87,101]. Absorption peaks of Cu impurity were observed in ZnTe crystals grown by traveling heater method (THM) but were not observed in the ZnTe grown by PVT technique and the spectra of the Cu absorption peaks were interpreted on the basis of crystal field theory with a dynamic Jahn-Teller interaction acting on the excited states [101].

4. Chemical analysis. Spark source mass spectrographic (SSMS) analysis and atomic absorption (AA) spectrophotometry are the conventional and reliable, although destructive, methods for the impurity analysis. A comparison of the impurity levels in the ZnTe crystals grown by PVT and THM together with the results for a CdTe crystal grown by PVT are given in Table 8.

5. Synchrotron white beam X-ray topography (SWBXT). An overall mapping of the structural defects in a crystal wafer can be easily provided by the SWBXT technique. Recently, (111) wafers sliced from a ZnTe crystal grown by PVT were characterized by this technique [87,102,103]. A topography image in the transmission mode, as shown in Figure 31, revealed the presence of dislocation slip bands, subgrain structures and long, thin 180° rotational twin lamella. The cellular dislocation structures comprise small-angle subgrain boundaries with a dislocation density around 10^5-10^6 cm^{-2} and a lower dislocation density in the 10^3 cm^{-2} range existing within the subgrains. The initiation of slip at regions of stress concentration, such as the lateral twin boundaries, the junctions of subgrain boundaries and twin boundaries was also revealed. The chronological growth history of the crystal and the possible mechanisms for the production of a long, thin twin lamella were deduced from the SWBXT images of a series of wafers sliced from one ZnTe crystal [103]. The SWBXT images of the ZnSe wafers have different features from that observed on the ZnTe wafers. Although long, thin twins were still present, instead of the cellular subgrain structure the SWBXT images of the ZnSe wafers show network of slip bands along three (111) slip planes.

Table 8. Chemical analysis of PVT and THM grown ZnTe and PVT grown CdTe by spark source mass spectroscopy (in parts per billion, atomic).

Element	ZnTe (THM-1)	ZnTe (PVT)	ZnTe[a] (THM-2)	CdTe (PVT)
Li	3	2	2	2
Na	5	3	5	3
Al	50	50	30	30
Si	500	300	300	300
P	30	20	<20	<20
S	[b]	[b]	[b]	3000
Cl	<50	<50	<50	<10
K	3	2	<2	5
Ca	50	30	<20	50
Cr	20	<10	<10	20
Fe	200	100	50	[b]
Cu	100[c]	50[c]	100[c]	<500
Se	200	100	30	100
In	<300	<300	<300	1000

a. Sublimed ZnTe was used as starting material.
b. Interference from matrix elements.
c. Determined by atomic absorption spectroscopy. SSMS values were <3000 ppba.

6. Photoluminescence (PL). The presence of Cu impurity, as a substitutional acceptor, was also confirmed by PL measurements at 10.6 K [104] in the ZnTe crystals grown by both PVT and THM. The THM ZnTe crystals were found to contain more Cu impurity than the PVT ZnTe crystals as one would expect from the purification function of the PVT process. The formation of Cu_{Zn}-V_{Te} complexes and the effects of annealing, oxygen contamination and intentional Cu doping were also studied [104]. The effects of post-growth annealing of CdS crystals in Cd and S over pressures were also investigated by PL on two types of

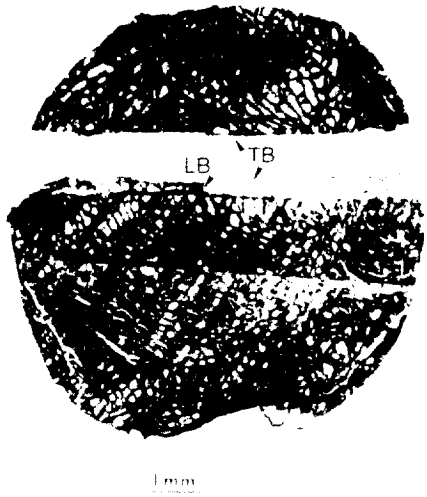

Figure 31. A SWBXT image of a (111) ZnTe wafer grown by PVT. TB — twin boundary; LB — lateral twin boundary.

as-grown crystals, one "dark" and the other "clear" and a model for the mechanism of the native defect formation was discussed [105].

VIII. Discussion

Both theoretical and experimental results demonstrate the importance of the control in the starting material stoichiometry to the transport rate and consequently the growth process. The heat treatment of the starting materials discussed here provides starting materials with a reproducible stoichiometry. However, the transport rate can also be limited by the residual gas pressure. The analysis of the composition of the residual gas implies that the potential source of the carbon and oxygen observed in the residual gas was the starting materials. The heat treatment process of flowing hydrogen over the source materials at elevated temperature can reduce the oxygen content, lower the residual gas pressure and, consequently, increase the growth rate.

In-situ measurements, such as the simultaneous measurements of partial pressures and the transport rates described, has furthered our understandings of the vapor species transport mechanism. On the other hand, the issues on the growth process and the kinetics at the growth interface such as how do the group VI dimers decompose into atoms, how is the molecular structure formed, what are the effects of the surface diffusion and re-vaporization of material on the forming of crystals and, consequently, what are the effects of surface morphology in the atomic scale on the kinetics and the crystallization process of the crystals, etc., have not been understood at this time. However, in the (3×1) reconstruction of the CdTe (001) surface stabilized by Te atoms, formation of surface Te dimers and the presence of vacancies were observed in the study of high-resolution electron microscopy [106]. The influence of substrate orientation on the growth kinetics of chemical vapor deposition of GaAs/GaAs has been widely investigated. Since the differences in the growth rate for different surface orientations exist mainly in the low temperature region it was concluded by Shaw [107] that the process is mass transfer limited at high temperatures and kinetically limited at low temperatures and in this low temperature region the growth rate minima were found on those orientations corresponding to the densely packed surfaces. The deposition rates in the epitaxial growth of ZnSe on GaAs vary from 0.2 μm/h on a (111)A substrate to 0.5 μm/h on a (111)B and 0.97 μm/h on a (112) substrate [75]

implies that not only the surface morphology but also the surface chemistry is playing a role in the deposition kinetics. The origin of the commonly observed 180° rotating twins in ZnTe and ZnSe grown crystals was not known. In the vapor phase epitaxy (basically, seeded PVT) growth of CdTe on CdTe substrates Yasushi et al. [108] found that twinned crystals of CdTe only grow on (111) substrates and do not grow on (211) surfaces and they speculated as follows. A (211) plane in a macroscopic sense consists of many (111) planes with steps between them and these steps define the atomic arrangement of the adsorbed molecules uniquely so that grown layers do not give twin crystals. On the other hand, the growth on the (111) face is a two-dimensional nucleation process and the nuclei can have two opposite orientations because of the freedom in rotation which results in twinning in the grown crystals. More elaborate research and investigation are needed to confirm the speculation. In-situ technique used in the MBE and MOCVD thin film technology to monitor the surface of growing crystals, when modified to fit into the high temperature and high pressure environment of the PVT process, will provide important information in the kinetics and process of the growth and formation of crystal and the mechanism of defect formation.

Acknowledgments

This work was supported by the Microgravity Science and Application Division of the National Aeronautics and Space Administration. The authors wish to thank the following persons for their contribution to the project: M. P. Volz, W. Palosz, D. C. Gillies, F. R. Szofran and S. L. Lehoczky at NASA/ Marshall Space Flight Center, Prof. R. F. Brebrick and his group at Marquette University, Prof. M. Dudley and his group at University of New York at Stony Brook and A. Burger and his colleagues at Fisk University.

REFERENCES:

[1] for example: Morkoc, H., Strite, S., Gao, G. B., Lin, M.E., Sverdlov, B. & Burns, M. 1994, J. Appl. Phys. 76, 1363; Krasnov, A. N., Purtov, Yu. N., Vaksman, Yu. F. & Serdyuk, V. V. 1992, J. Crystal Growth 125, 373; Kukimoto, H. 1991, Semicond. Sci. Technol. 6, A14.

[2] for example: Yang, X. H., Hays, J. M., Shan, W., Song, J. J. & Cantwell, E. 1993, Appl. Phys. Lett. 62, 1072; Jeon, H., Ding, J., Nurmikko, A. V., Xie, W., Grillo, D. C., Kobayashi, M., Gunshor, R. L., Hua, G. C. & Otsuka, N. 1992, Appl. Phys. Lett. 60, 2045; Nakanishi, K., Suemune, I., Fujii, Y., Kuroda, Y. & Yamanishi, M. 1991, Appl. Phys. Lett. 59, 1401; Neumark, G. F., Park, R. M. & Depuydt J. M. 1994, Physics Today, June, 26; Daneu, V., DeGloria, D. P., Sanchez, A., Tong, F. & Osgood, Jr. R. M. 1986, Appl. Phys. Lett. 49, 546.

[3] Howie, J. A. B., Rowles, G. K. & Hawkins, P. 1991, Meas. Sci. Technol. 2, 1070.

[4] for example: Yang, X. H., Hays, J., Shan, W., Song, J. J., Cantwell, E. & Aldridge, J. 1992, Appl. Phys. Lett. 60, 926; Jeon, H., Ding, J., Patterson, W., Nurmikko, A. V., Xie, W., Grillo, D. C., Kobayashi, M. & Gunshor, R. L. 1991, Appl. Phys. Lett. 59, 3619.

[5] Ichino, K., Wu, Y.-H., Kawakami, Y., Fujita, S. & Fujita, S. 1992, J. Crystal Growth 117, 527.

[6] Triboulet, R. 1991, Semicon. Sci. Technol. 6, A18.

[7] Carides, J. & Fischer, A. G. 1964, Solid State Commun. 2, 217.

[8] Sato, K. & Adachi, S. 1993, J. Appl. Phys. 73, 926.

[9] Sysoev, L. A., Raiskin, E. K. & Gur'ev, V. R. 1967, Inorg. Mater. 3, 341.

[10] Tai, H., Nakajima, S. & Hori, S. 1976, J. Japan. Inst. Metals 40, 474.

[11] Ebina, A., Fukunaga, E. & Takahashi, T. 1974, Phys. Rev. B10, 2495.

[12] Lauck, R., Muller-Vogt, G. & Wendl, W. 1986, J. Crystal Growth 74, 520.

[13] for example: Chernov, A. A., 1974, J. Crystal Growth 24/25, 11; Rosenberger, F., Delong, M. C., Greenwell, D. W., Olson, J. M. & Westphal, G. H. 1975, J. Crystal Growth 29, 49; Xiao, R.-F., Alexander, J. I. & Rosenberger, F. 1990, J. Crystal Growth 100, 313.
[14] Chen, J.-S., Ming, N.-B., Rosenberger, F. 1986, J. Chem. Phys. 84, 2365.
[15] Sharma, R. C. & Chang, Y. A. 1988, J. Crystal Growth 88, 193.
[16] Sha, Y.-G., Su, C.-H., Palosz, W., Volz, M. P., Gillies, D. C., Szofran, F. R., Lehoczky, S. L., Liu, H.-C. & Brebrick, R. F., J. Crystal Growth, in press.
[17] Brebrick, R. F. 1969, J. Electrochem. Soc. 116, 1274.
[18] Goldfinger, P. & Jeunehomme, M. 1963, Trans. Faraday Soc. 59, 2851.
[19] Floegel, P. Z. 1969, Anorg. Allg. Chem. 370, 16.
[20] Brebrick, R. F. 1971, J. Electrochem. Soc. 118, 2014.
[21] Huang, Y. & Brebrick, R. F. 1988, J. Electrochem. Soc. 135, 486.
[22] Brebrick, R. F. & Strauss, A. J. 1964, J. Chem. Phys. 40, 3230.
[23] Northrop, D. A. 1971, J. Phys. Chem. 75, 118.
[24] Brebrick, R. F. & Strauss, A. J. 1964, J. Chem. Phys. 41, 197.
[25] Huang, Y. & Brebrick, R. F. 1988, J. Electrochem. Soc. 135, 1547.
[26] JANAF Thermochemical Tables, 1971, NSRDS-NBS, Natl. Bur. Std. (US), Washington, DC, 2nd ed.; Piechotka, M. & Kaldis, E. 1986, J. Less Common Metals 115, 315.
[27] Cadoret, R., Brisson, P. & Magnan, A. 1989, Nucl. Inst. Meth. A283, 339.
[28] Klosse, K. & Ullersma, P. 1973, J. Crystal Growth 18, 167.
[29] Faktor, M. M. & Garrett, I. 1974, Growth of Crystals from the Vapour, Chapman and Hall, London.
[30] Su, C.-H. 1987, J. Crystal Growth 80, 333.
[31] Reid, R. C., Prausnitz, J. M. & Sherwood, T. K. 1977, The Properties of Gases and Liquids, McGraw-Hill, New York, 3rd ed.
[32] Su, C.-H., Liao, P.-K., Huang, Y., Liou, S.-S. and Brebrick, R. F. 1984, J. Chem. Phys. 81, 11.
[33] Shteingradt, D. M. & Lyusternik, V. E. 1982, Russ. J. Phys. Chem. 56, 1379.
[34] Svehla, R. A. 1962, NASA Tech. Report R-132, Lewis Research Center, Cleveland, Ohio.
[35] Hirschfelder, J. O., Curtis, C. F. & Bird, R. B. 1954, Molecular Theory of Gases and Liquids, Wiley, New York.
[36] for example: Russell, G. J. & Woods, J. 1979, J. Crystal Growth 46, 323; Schmidt, G. & Gruehn, R. 1982, J. Crystal Growth 57, 585; Morimoto, Y., Igarashi, T., Sugahara, H. & Nasu, S. 1992, J. Non-Cryst. Solids 139, 35.
[37] Harman, T. C. & McVittie, J. P. 1974, J. Electron. Mater. 3, 843.
[38] Palosz, W. & Wiedemeier, H. 1993, J. Crystal Growth 131, 193.
[39] Palosz, W., Szofran, F. R. & Lehoczky, S. L. 1994, J. Crystal Growth 142, 215.
[40] Sherwood, T. K. 1937, Absorption and Extraction, McGraw-Hill, New York.
[41] Palosz, W. & Wiedemeier, H. 1993, J. Crystal Growth 129, 653.
[42] Palosz, W., Szofran, F. R. & Lehoczky, S. L., J. Crystal Growth, in press.
[43] Piper, W. & Polich, S. J. 1961, J. Appl. Phys. 32, 1278.
[44] Catano, A. & Kun, Z. K. 1976, J. Crystal Growth 33, 324.
[45] Kaldis, E. 1965, J. Phys. Chem. Solids 26, 1701.
[46] Ohno, T., Kurisu, K. & Taguchi, T. 1990, J. Crystal Growth 99, 737.
[47] Burr, K. F. & Woods, J. 1971, J. Crystal Growth 9, 183.
[48] Prior, A. C. 1961, J. Electrochem. Soc. 108, 82.

[49] Igaki, K., Ohashi, N. & Mochizuki, K. 1976, Jap. J. Appl. Phys. 15, 1429.
[50] Igaki, K. & Mochizuki, K. 1974, J. Crystal Growth 24/25, 162.
[51] Mochizuki, K. 1981, J. Crystal Growth 51, 453.
[52] Mochizuki, K. 1981, J. Crystal Growth 53, 355.
[53] Kiyosawa, T., Igaki, K. & Ohashi, N. 1972, Trans. Jap. Inst. Metals 13, 248.
[54] Hoschl, P. & Konak, C. 1965, Phys. Stat. Sol. 9, 167.
[55] Cutter, J. R. & Woods, J. 1979, J. Crystal Growth 47, 405.
[56] Clark, L. & Woods, J. 1968, J. Crystal Growth 3/4, 126.
[57] Cutter, J. R., Russell, G. J. & Woods, J. 1976, J. Crystal Growth 32, 179.
[58] Mochizuki, K. & Igaki, K. 1978, J. Crystal Growth 45, 218.
[59] Mochizuki, K. 1982, J. Crystal Growth 58, 87.
[60] Brebrick, R. F. & Strauss, A. J. 1965, J. Phys. Chem. Solids 26, 989.
[61] Su, C.-H., Liao, P.-K., Tung, T. & Brebrick, R. F. 1981, High Temp. Sci. 14, 181.
[62] Brebrick, R. F. 1965, J. Chem. Phys. 43, 3846.
[63] Schwartz, J. P., Tung, T. & Brebrick, R. F. 1981, J. Electrochem. Soc. 128, 438.
[64] Tung, T., Golonka, L. & Brebrick, R. F. 1981, J. Electrochem. Soc. 128, 451.
[65] Su, C.-H., Liao, P.-K. & Brebrick, R. F. 1985, J. Electrochem. Soc. 132, 942.
[66] Chen, K.-T., Sha, Y.-G. & Brebrick, R. F. 1990, J. Vac. Sci. Technol. A8, 1086.
[67] Murray, J. J., Pottie, R. F. & Sander, R. L. 1973, J. Mater. Sci. 8, 37.
[68] Morimoto, Y., Igarashi, T., Sugahara, H. & Nasu, S. 1992, J. Non-Cryst. Solids 139, 35.
[69] Zha, M., Piechotka, M. & Kaldis, E. 1991, J. Crystal Growth 115, 43.
[70] Kaldis, E. & Piechotka, M. 1994, Handbook of Crystal Growth, Vol. 2, Chap. 11, Elsevier Science, North-Holland.
[71] Zoutendyk, J. A. & Akutagawa, W. M. 1982, Mater. Processing in the Reduced Gravity Environment of Space, Elsevier Science, Rindone, G. E. Editor, p. 449.
[72] Wiedemeier, H., Chandra, D. & Klaessic, F. C. 1981, J. Crystal Growth 51, 345.
[73] Kaldis, E. 1969, J. Crystal Growth 5, 376.
[74] Parker, S. 1971, J. Crystal growth 9, 177.
[75] Koyama, T., Yodo, T., Oka, H., Yamashita, K. & Yamasaki, T. 1988, J. Crystal Growth 91, 639.
[76] Recker, K. & Schoepe, R. 1971, J. Crystal Growth 9, 189.
[77] Parker, S. G. & Pinnell, J. E. 1969, Trans. Meta. Soc. AIME 245, 451.
[78] Hartmann, H. 1977, J. Crystal Growth 42, 144.
[79] Fujita, S., Mimoto, H., Takebe, H. & Noguchi, T. 1979, J. Crystal Growth 47, 326.
[80] Russell, G. J. & Woods, J. 1979, J. Crystal Growth 47, 647.
[81] Morimoto, J., Ito, T., Yoshioka, T. & Miyakawa, T. 1982, J. Crystal Growth 57, 362.
[82] Markov, E. V. & Davydov, A. A. 1971, Neorg. Mater. 7, 575.
[83] Davydov, A. A. Ermolov, V. N., Neustroev, S. V. & Pavlova, L. P. 1992, Neorg. Mater. 28, 42.
[84] Cantwell, G., Harsch, W. C., Cotal, H. L., Markey, B. G., McKeever, S. W. S. & Thomas, J. E. 1992, J. Appl. Phys. 71, 2931.
[85] Hemmat, N. & Weinstein, M. 1967, J. Electrochem. Soc. 114, 851.
[86] Su, C.-H., Lehoczky, S. L. & Szofran, F. R. 1990, J. Crystal Growth 101, 221.
[87] Su, C.-H., Volz, M. P., Gillies, D. C., Szofran, F. R., Lehoczky, S. L., Dudley, M., Yao, G.-D. & Zhou, W. 1993, J. Crystal Growth 128, 627.
[88] Taguchi, T., Fujita, S. & Inuishi, Y. 1978, J. Crystal growth 45, 204.
[89] Anderson, E., Cheng, H.-Y. & Edgell, M. J. 1989, Mater. Res. Soc. Symp. Proc. 152, 51.
[90] Cheng, H.-Y. & Anderson, E. 1989, J. Crys-

tal Growth 96, 756.
[91] Allegretti, F., Carrara, A. & Pizzini, S. 1993, J. Crystal Growth 128, 646.
[92] Su, C.-H., Sha, Y.-G., Volz, M. P., Gillies, D. C., Szofran, F. R., Lehoczky, S. L., Zhou, W., Dudley, M., Liu, H.-C., Brebrick, R. F. & Wang, J. C. 1994, Proc. AIAA 32nd Aerospace Sciences Meeting, paper 94-0564.
[93] Russell, G. J., Thompson, N. F. & Woods, J. 1985, J. Crystal Growth 71, 621.
[94] Fochs, P. D., George, W. & Augustus, P. D. 1968, J Crystal Growth 3/4, 122.
[95] Hartmann, H. & Siche, D. 1994, J. Crystal Growth 138, 260.
[96] Grasza, K., Zuzga-Grasza, U., Jedrzejczak, A., Galazka, R. R., Majewski, J., Szadkowski, A. & Grodzicka, E. 1992, J. Crystal Growth 123, 519.
[97] Jordan, A. S. & Derick, L. 1969, J. Electrochem. Soc. 116, 1424.
[98] Sha, Y.-G., Su, C.-H. & Szofran, F. R. 1993, J. Crystal Growth 131, 574.
[99] Chen, K.-T., George, M. A., Zhang, Y., Burger, A., Su, C.-H., Sha, Y.-G., Gillies, D. C. Gillies & Lehoczky, S. L., J. Crystal Growth, in press.
[100] for example: Su, C.-H., Perry, G. L. E., Szofran, F. R. & Lehoczky, S. L. 1988, J. Crystal Growth 91, 20; Su, C.-H., Lehoczky, S. L. & Szofran, F. R. 1991, J. Crystal Growth 109, 392.
[101] Volz, M. P., Su, C.-H., Lehoczky, S. L. & Szofran, F. R. 1992, Phys. Rev. B46, 76.
[102] Zhou, W., Wu, J., Dudley, M., Su, C.-H., Volz, M. P., Gillies, D. C., Szofran, F. R. & Lehoczky, S. L. 1993, Mater. Res. Soc. Symp. Proc., Infrared Detectors-Materials, Processing, and Devices, Applebaum, A. & Dawson, L. R., Editors, p. 299.
[103] Zhou, W., Dudley, M., Wu, J., Su, C.-H., Volz, M. P., Gillies, D. C., Szofran, F. R. & Lehoczky, S. L. 1994, Mater. Sci. & Eng. B27, 143.
[104] Biao, Y., Azoulay, M., George, M. A., Burger, A., Collins, W. E., Silberman, E., Su, C.-H., Volz, M. E., Szofran, F. R. & Gillies, D. C. 1994, J. Crystal Growth 138, 219.
[105] Chen, K.-T., Zhang, Y., Egarievwe, S. U., George, M. A., Burger, A., Su, C.-H., Sha, Y.-G. & Lehoczky, S. L., submitted to the 11th International Conference on Crystal Growth (ICCG XI), The Hague, The Netherland, June 18-23, 1995.
[106] Lu, P. and Smith, D. J. 1991, Surface Sci. 254, 119
[107] Shaw, D. W 1975, J. Crystal Growth 31, 130.
[108] Yoshioka, Y., Yoda, H. & Kasuga, M. 1991, J. Crystal Growth 115, 705.